Journal of Medicinal Chemistry

Article

pubs.acs.org/jmc

Structure−Activity Profiles of Novel 6-Substituted Pyrrolo[2,3-*d*]pyrimidine Thienoyl Antifolates with Modified Amino Acids for Cellular Uptake by Folate Receptors α and β and the Proton-Coupled Folate Transporter

Lalit K. Golani,[†] Christina George,[‡] Sai Zhao,[†] Sudhir Raghavan,[†] Steven Orr,[‡] Adrianne Wallace,[‡] Mike R. Wilson,[§] Zhanjun Hou,[‡] Larry H. Matherly,*[,‡,§,∥,⊥] and Aleem Gangjee*[,†,⊥]

[†]Division of Medicinal Chemistry, Graduate School of Pharmaceutical Sciences, Duquesne University, 600 Forbes Avenue, Pittsburgh, Pennsylvania 15282, United States

[‡]Molecular Therapeutics Program, Barbara Ann Karmanos Cancer Institute, 110 East Warren Avenue, Detroit, Michigan 48201, United States

[§]Cancer Biology Graduate Program, Department of Oncology, Wayne State University School of Medicine, Detroit, Michigan 48201, United States

[∥]Department of Pharmacology, Wayne State University School of Medicine, Detroit, Michigan 48201, United States

Supporting Information

ABSTRACT: Structure−activity relationships for cellular uptake and inhibition of cell proliferation were studied for 2-amino-4-oxo-6-substituted pyrrolo[2,3-*d*]pyrimidine thienoyl antifolates in which the terminal L-glutamate of the parent structure (**7**) was replaced by natural or unnatural amino acids. Compounds **7** and **10**−**13** were selectively inhibitory toward folate receptor (FR) α-expressing Chinese hamster ovary (CHO) cells. Antiproliferative effects of compounds **7** and **9**−**13** toward FRα- and FRβ-expressing CHO cells were only partly reflected in binding affinities to FRα and FRβ or in the docking scores with molecular models of FRα and FRβ. Compounds **7** and **11** were potent inhibitors of glycinamide ribonucleotide formyltransferase in de novo purine biosynthesis in KB human tumor cells. These studies establish for the first time the importance of the α- and γ-carboxylic acid groups, the length of the amino acid, and the conformation of the side chain for transporter binding and biological activity of 6-substituted pyrrolo[2,3-*d*]pyrimidine thienoyl antifolates.

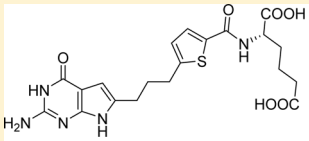

11 FRα IC_{50} (RT16 cells) = 9.5 nM
GARFTase IC_{50} = 12 nM

Distinct docked conformations of **11** in GARFTase and FRα, different from its energy minimized conformation.

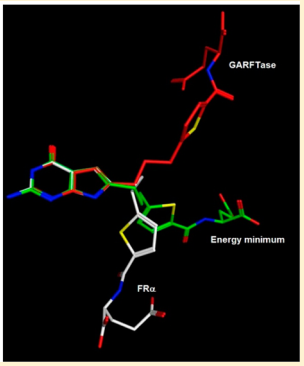

INTRODUCTION

Membrane transport of folates and classical antifolates is mediated by the reduced folate carrier (RFC or SLC19A1), the proton-coupled folate transporter (PCFT or SLC46A1), and folate receptors (FRs) α and β.[1−5] RFC is ubiquitously expressed in tissues and tumors and is an anion antiporter that functions optimally at neutral pH.[2] PCFT shows more limited expression in normal tissues than RFC but is highly expressed in the duodenum and jejunum as well as in liver and kidney.[4] PCFT is widely expressed in human tumors and shows optimal transport at acidic pH with very low activity at neutral pH.[4,6] High levels of FRs are expressed in certain cancers, including FRα in ovarian and nonsmall cell lung cancers and FRβ in myeloid leukemias.[1,7]

Folate-based drugs continue to occupy an important niche among current chemotherapy drugs for cancer and nonmalignant diseases.[4,5,8−10] Clinically relevant antifolates include methotrexate (MTX) and pralatrexate, both of which inhibit dihydrofolate reductase, and raltitrexed (RTX) and pemetrexed (PMX), which principally inhibit thymidylate synthase (Figure 1). Recent attention has focused on developing tumor-targeted folate-based therapies, reflecting tumor-selective uptake by FRs and/or PCFT.[4,5,10] Folate and pteroate conjugates have been used to selectively deliver toxins, liposomes, and cytotoxic agents via FRα to FRα-expressing tumors.[10] Vintafolide, a folic acid−desacetyl vinblastine conjugate and substrate for FRα,[11] completed a phase II multicenter randomized trial for women with platinum-resistant ovarian cancer[12] and was tested in phase III clinical trials with patients with ovarian and nonsmall cell lung cancers.

PMX is a 5-substituted 2-amino-4-oxo-pyrrolo[2,3-*d*]-pyrimidine analogue with a two-carbon bridge attached to a *p*-aminobenzoyl glutamate (Figure 1). We previously identified

Received: July 22, 2014
Published: September 19, 2014

   dx.doi.org/10.1021/jm501113m | *J. Med. Chem.* 2014, 57, 8152−8166

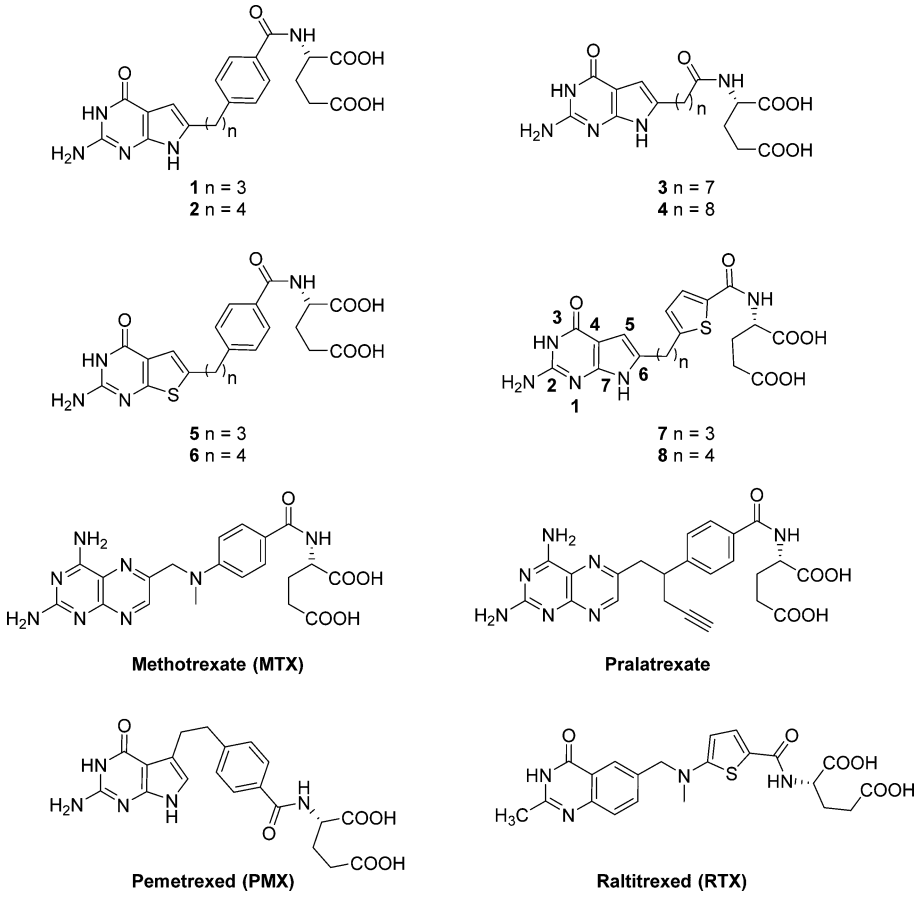

Figure 1. Folate receptor- and PCFT-targeted antifolates **1**–**8** and clinically relevant antifolates, methotrexate (MTX), pemetrexed (PMX), pralatrexate, and raltitrexed (RTX).

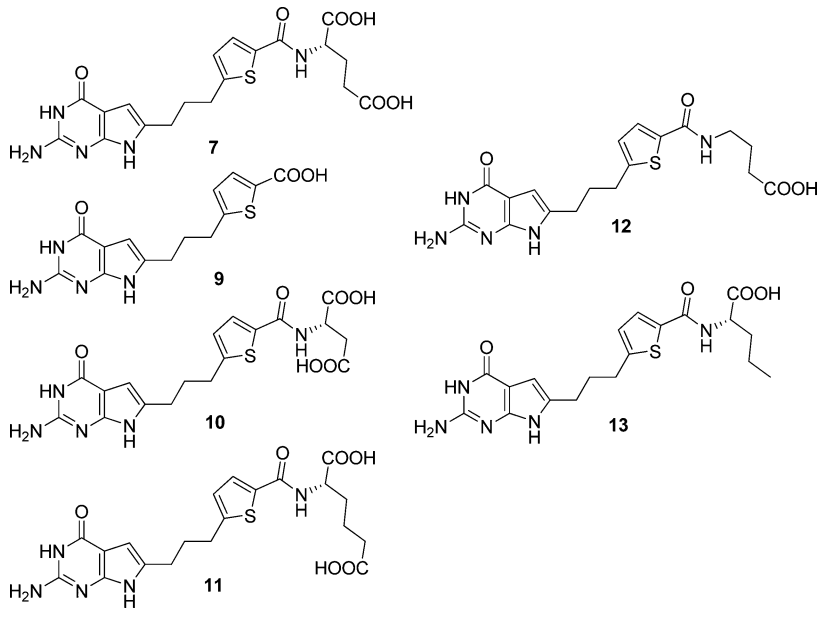

Figure 2. Structures of compounds **7** and **9**–**13**.

novel 6-substituted pyrrolo[2,3-*d*]pyrimidine analogues of PMX with selective cellular uptake by FRα and β and PCFT over RFC.[13,14] The most potent cytotoxic analogues that utilize both FR and PCFT were those with three or four carbons in the bridge region (**1** and **2**) (Figure 1; Table 1S, Supporting Information); inhibitory activity for this series decreased dramatically with fewer or greater numbers of bridge carbons.[13,14] However, replacement of the benzoyl ring with an alkyl side chain (n = 7 or 8) (**3** and **4**) (Figure 1) preserved substantial FR substrate activity and growth inhibitory effects, although PCFT transport was lost (Table 1S, Supporting Information).[15] Substitution of the pyrrole ring in **1** and **2** with

dx.doi.org/10.1021/jm501113m | J. Med. Chem. 2014, 57, 8152–8166

Scheme 1[a]

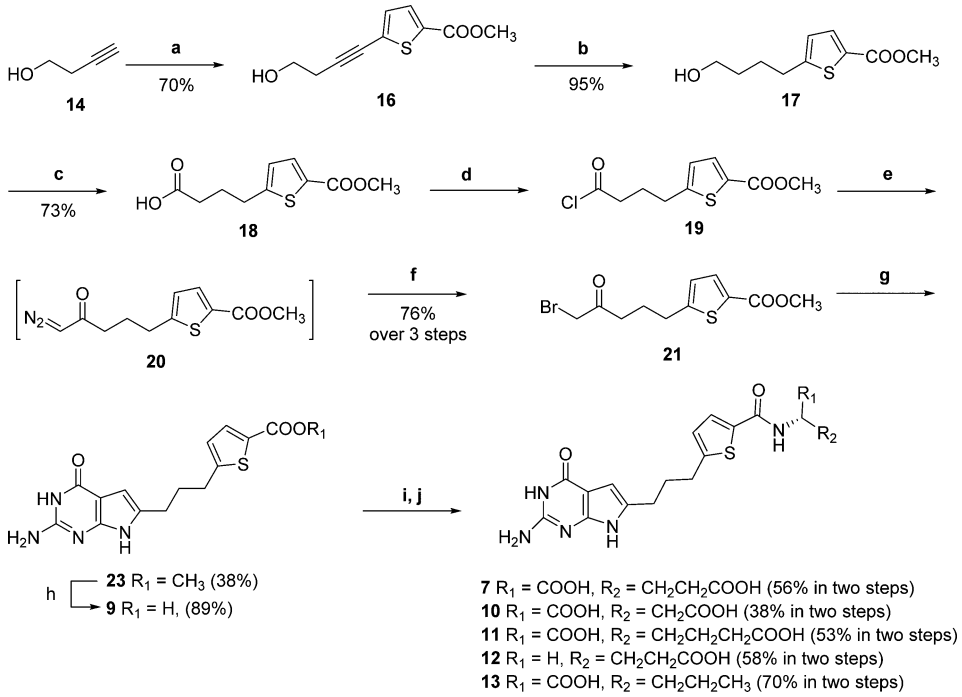

[a]Reagents and conditions: (a) 5-bromo-thiophene-2-carboxylic acid methyl ester (**15**), CuI, $PdCl_2$, PPh_3, Et_3N, CH_3CN, microwave, 100 °C, 10 min; (b) 10% Pd/C, H_2, 55 psi, MeOH, 2 h; (c) H_5IO_6, PCC, 0 °C to RT, 3 h; (d) oxalyl chloride, CH_2Cl_2, reflux, 1 h; (e) diazomethane, Et_2O, rt, 1 h; (f) HBr, 70−80 °C, 2 h; (g) 2,4-diamino-6-hydroxypyrimidine (**22**), DMF, rt, 3 days; (h) (i) 1N NaOH, RT, 12 h, (ii) 1 N HCl; (i) *N*-methylmorpholine, 2-chloro-4,6-dimethoxy-1,3,5-triazine, L-glutamate diethyl ester hydrochloride or dimethyl L-aspartate or dimethyl (*S*)-2-aminohexanedioate or methyl 4-aminobutyrate hydrochloride or methyl (*S*)-2-aminopentanoate, DMF, RT, 12 h; (j) (i) 1N NaOH, rt, 12 h, (ii) 1 N HCl.

a thiophene ring afforded a somewhat larger ring system, while replacing the NH hydrogen bond donor with S (**5** and **6**)[16] (Figure 1). Compounds **5** and **6** were excellent substrates for FRs, resulting in growth inhibition equivalent to **1** and **2**, but were not substrates for transport by RFC and PCFT.[16] The 6-substituted pyrrolo[2,3-*d*]pyrimidine analogues with a side chain thienoyl-for-benzoyl isostere replacement in **1** and **2** afforded the most active FR- and PCFT-selective antifolates yet discovered (**7** and **8**, respectively) (Figure 1; Table 1S, Supporting Information).[17−20] For **7**, cell growth inhibition compared to **8** was increased up to ∼10-fold toward FRα- and PCFT-expressing tumor cells.[18] All the active 6-substituted pyrrolo[2,3-*d*]pyrimidine antifolates evaluated thus far derived their cell inhibitory effects from inhibition of β-glycinamide ribonucleotide (GAR) formyltransferase (GARFTase) which catalyzes the first folate-dependent step in de novo purine nucleotide biosynthesis.[17−20]

Further structural optimization of compounds such as **7**, for which drug efficacy depends on selective cellular uptake by non-RFC transport mechanisms, and binding to folylpolyglutamate synthase for polyglutamylation and GARFTase to inhibit purine nucleotide biosynthesis, requires a systematic variation of individual structural features.

For example, although compound **7** is highly potent, its selective tumor-targeting via FRs and PCFT is somewhat compromised by its apparent cellular uptake by other processes.[18] Thus, it is of interest to further explore the structure−activity relationships (SAR) for this series to determine if absolute selectivity along with high potency for FRα, FRβ, and/or PCFT over RFC would be possible. In this report, we consider the SAR for cellular uptake and inhibition of cell proliferation for the pyrrolo[2,3-*d*]pyrimidine scaffold of **7** in which the terminal L-glutamate has been replaced by natural or unnatural amino acids with variations in the length of the side chain or the presence of α- or γ-COOH groups or deleted altogether. Our goal was to explore the SAR for novel 6-substituted pyrrolo[2,3-*d*]pyrimidine thienoyl antifolates **9**−**13** related to **7** (Figure 2), the most potent compound of our series for inhibiting proliferation of FRα- and PCFT-expressing cells with substantially reduced inhibitory effects toward RFC-expressing cells.[18]

Using the pyrrolo[2,3-*d*]pyrimidine scaffold, we systematically modified the terminal glutamate moiety. Compound **9** is the pteroic acid analogue of **7** in which the terminal L-glutamate portion is removed. Compound **10** contains a single carbon-truncated L-glutamate, i.e., an aspartic acid analogue of compound **7**. Compound **11** contains an extended 3-atom amino acid side chain, i.e., the α-amino adipic acid analogue of compound **7**. Compound **12**, the 4-amino butanoic acid analogue, lacks an α-carboxylic acid compared with **7**. Compound **13** includes an α-amino pentanoic acid that lacks a γ-carboxylic acid. Collectively, these analogues allow the determination of the importance of the α- and γ-carboxylic acid groups and the length of the side chain of the L-glutamate moiety in relation to biological activity for FR and PCFT targeting. Our results establish an intriguing difference between the amino acid specificities for binding FRα and FRβ, and biological effects between analogues of this series, and in conformational preferences for optimal binding to FRα and GARFTase that may be therapeutically exploitable. Thus, a degree of flexibility in the amino acid side chain appears to be

dx.doi.org/10.1021/jm501113m | *J. Med. Chem.* 2014, 57, 8152−8166

Table 1. IC50s (in nM) for 6-Substituted Pyrrolo[2,3-*d*]pyrimidine Antifolates and Classical Antifolates in RFC-, PCFT-, and FR-Expressing Cell Lines[a]

	RFC		FRα		FRβ		PCFT		RFC/FRα/PCFT	
compd	PC43-10	R2	RT16	RT16 (+FA)	D4	D4 (+FA)	R2/PCFT4	R2 (VC)	KB	KB (+FA)
7	101.0(16.6)	273.5(49.1)	0.31(0.14)	>1000	0.17(0.03)	>1000	3.34(0.26)	288(12)	0.26 (0.03)	>1000
9	>1000	>1000	661(170)	>1000	>1000	>1000	>1000	>1000	>1000	>1000
10	>1000	>1000	6.6(1.9)	>1000	347(110)	>1000	>1000	>1000	>1000	>1000
11	>1000	>1000	9.5 (1.9)	>1000	3.6 (0.6)	>1000	>1000	>1000	9.0 (5.0)	>1000
12	>1000	>1000	27.4 (12.2)	>1000	>1000	>1000	>1000	>1000	>1000	>1000
13	>1000	>1000	55.7(7.9)	>1000	>1000	>1000	>1000	>1000	>1000	>1000
MTX	12(1.1)	216(8.7)	114(31)	461(62)	106(11)	211(43)	120.5(16.8)	>1000	6.0(0.6)	20(2.4)
PMX	138(13)	894(93)	42(9)	388(68)	60(8)	254(78)	13.2(2.4)	974.0(18.1)	68(12)	327(103)
RTX	6.3(1.3)	>1000	15(5)	>1000	22(10)	746(138)	99.5(11.4)	>1000	5.9(2.2)	22(5)

[a]Growth inhibition assays were performed for CHO sublines engineered to express human RFC (PC43-10), FRα (RT16), FRβ (D4), or PCFT (R2/PCFT4), for comparison with transporter-null [R2, R2(VC)] CHO cells, and for the KB human tumor subline (expresses RFC, FRα, and PCFT), as described in the Experimental Section. For the FR experiments, growth inhibition assays were performed in the presence and the absence of 200 nM folic acid (FA). The data shown are mean values from 3−10 experiments (plus/minus SEM in parentheses). Results are presented as IC_{50} values, corresponding to the concentrations that inhibit growth by 50% relative to cells incubated without drug. Data for compound **7**, MTX, PMX, and RTX were previously published.[13,16−18,23] The structures for the classical antifolate drugs are shown in Figure 1 and those for compounds **7** and **9**−**13** in Figure 2. ND: not determined.

essential to provide both selective transport and potent enzyme inhibition.

CHEMISTRY

Target compounds **7**, **9**, and **10**−**13** were synthesized from **17** (Scheme 1).[17] Previously reported intermediate **17** was oxidized using Jones reagent,[17] which afforded the carboxylic acid **18** in 47% yield. Because **17** was a key intermediate, it was of interest to improve the oxidation yield so milder oxidation conditions were used than Jones reagent. Compound **17** was oxidized using periodic acid and pyridinium chlorochromate, which afforded **18** in significantly improved (73%) yield over the previous method. Intermediate **18** was converted to the acid chloride **19** and immediately reacted with diazomethane, followed by 48% HBr to give the desired α-bromomethylketone **21**. Condensation of 2,6-diamino-3*H*-pyrimidin-4-one (**22**) with **21** at room temperature for 3 days afforded the 2-amino-4-oxo-6-substituted-pyrrolo[2,3-*d*]pyrimidine **23** (38%). Hydrolysis of **23** gave the corresponding free acid **9** (89%).[17] Subsequent coupling with L-glutamate diethyl ester or dimethyl L-aspartate or dimethyl (*S*)-2-aminohexanedioate, methyl 4-aminobutanoate, or methyl (*S*)-2-aminopentanoate, using 2-chloro-4,6-dimethoxy-1,3,5-triazine as the activating agent, afforded the desired esters. Final saponification of the esters gave the desired compounds, **7** and **10**−**13**, in 78−89% yield.

BIOLOGICAL EVALUATION AND DISCUSSION

6-Substituted Pyrrolo[2,3-*d*]pyrimidine Antifolates with Amino Acid Replacements Are Inhibitors of Proliferation of Cells Expressing FRs but Not PCFT or RFC. Compounds **9**−**13** were tested in cell proliferation assays with a unique panel of isogenic Chinese hamster ovary (CHO) cell lines individually expressing RFC (PC43-10),[13,21] PCFT (R2/PCFT4),[14,16] FRα (RT16),[13] or FRβ (D4),[16] and results were compared to those for **7** and to standard antifolates (MTX, PMX, RTX) with limited transporter selectivity. Negative controls for RFC- and PCFT-expressing cells included RFC-, FR-, and PCFT-null MTXRIIOua^{R}2-4 (R2) CHO cells[22] [either the parental R2 subline or vector control R2(VC) cells, with identical results (see Experimental Section)]; for the FR-expressing CHO cells, cells were treated with excess folic acid (200 nM) to block cellular uptake by FR as a negative control. The experiments with the CHO sublines were extended to KB human nasopharengeal carcinoma cells which express highly elevated FRα, along with RFC and PCFT.[19] Results are summarized in Table 1.

Compound **7** is extraordinarily potent toward both FR and PCFT-expressing CHO cells (IC_{50}s = 0.31, 0.17, and ∼3 nM for RT16, D4, and R2/PCFT4, respectively) and KB human tumor cells (IC_{50} = 0.26 nM).[18] Compound **7** showed modest inhibition toward PC43-10 and R2 cells that was unrelated to the presence of a particular transporter (Table 1). Removal of the terminal glutamate of **7**, generating **9**, resulted in complete loss of growth inhibition toward RFC- and PCFT-expressing CHO cells and only a slight inhibition (IC_{50} = 661 nM) of FRα-expressing RT16 cells. Compound **9** was completely inactive with FRβ-expressing D4 CHO cells. For PC43-10 (RFC) and R2/PCFT4 (PCFT) cells, the analogues with amino acid replacements including **10**−**13** were all inactive up to 1000 nM. In contrast, compounds **10**−**13** were all inhibitory toward RT16 cells at low nM concentrations, in rank order, **10** ∼ **11** > **12** > **13**. Interestingly, for FRβ-expressing D4 cells, only **11** was highly active (IC_{50} = 3.6 nM), with substantially reduced activity for **10** and complete inactivity with **12** and **13**. For all the active compounds with both RT16 and D4 cells, growth inhibition was reversed by excess folic acid, confirming FR uptake. As previously reported,[13,16−18,23] transporter selectivity was lost for the classical antifolates (MTX, PMX, RTX), as all these agents inhibited proliferation of FR-, RFC-, and PCFT-expressing CHO cells (Table 1).

Thus, on the basis of the patterns of inhibition with the isogenic CHO sublines, L-glutamate replacements in **7** preserve substantial FRα-selective uptake and growth inhibition, with generally reduced and surprisingly variable activity for FRβ and a complete loss of RFC- and PCFT-targeted activity. Because compounds **10**−**13** all inhibited FRα-containing CHO cells, their inability to inhibit RFC- and PCFT-expressing CHO cells (and FRβ-expressing D4 cells for compounds **10**, **12**, and **13**) must be due to a lack of internalization by these mechanisms.

Notably, in spite of the inhibitory effects of **10**−**13** toward FRα-expressing RT16 CHO cells, with KB human tumor cells, the only active compound of the series was the adipic acid

dx.doi.org/10.1021/jm501113m | *J. Med. Chem.* 2014, 57, 8152−8166

analogue, **11**. With KB cells, **11** showed an IC_{50} of 9 nM; however, this was approximately 35-fold reduced from the very low IC_{50} (0.26 nM) measured with **7**. Thus, although these results with RT16 and KB cells clearly indicate that L-glutamate is optimal for FRα-targeted uptake of 6-pyrrolo[2,3-*d*]-pyrimidine thienoyl antifolates, unlike compound **7** the adipic acid analogue **11** has absolute selectivity for FRα and β with no uptake by other (mediated or nonmediated) processes. This increased selectivity of **11** over **7** for FR over nonmediated processes might be expected to translate into reduced in vivo toxicity, thereby providing a potential unexpected benefit.

Binding of Novel 6-Pyrrolo[2,3-*d*]pyrimidine Analogues with Modified Amino Acids to FRα and PCFT. Inhibition of proliferation of RT16 cells by compounds **9**−**13** was abolished by excess folic acid (Table 1), establishing an important role for FRα-mediated cellular uptake of these compounds. Analogous results were obtained with FRβ with compound **11**, although antiproliferative activity was substantially reduced with FRβ for compounds **9**, **10**, **12**, and **13**.

We used competitive [^{3}H]folic acid binding assays at 4 °C[13,16] to further establish binding of the novel analogues of **7** to FRα and FRβ in an attempt to provide a possible explanation for differences in drug efficacies between FRα- and FRβ-expressing cells. To determine relative affinities for FR binding, unlabeled pyrrolo[2,3-*d*]pyrimidine compounds **7** and **9**−**13** were each tested for their abilities to compete with [^{3}H]folic acid for binding to FRα in RT16 cells and to FRβ in D4 cells compared to unlabeled folic acid (positive control) and MTX (negative control). Cells were rinsed with acid-buffered saline to remove FR-bound folates. Cells were then incubated with [^{3}H]folic acid (50 nM) in the presence of unlabeled (anti)folate competitors (0−1000 nM). After further washing (neutral pH), cell proteins were solubilized with alkali, and FR-bound [^{3}H]folic acid was quantified and normalized to total cell proteins. Relative affinities were expressed as inverse molar ratios of (anti)folates required to decrease bound [^{3}H]folic acid by 50%, for which folic acid was assigned a value of 1[13,16] (Figure 3).

Disparate results were obtained for binding affinities of the novel 6-pyrrolo[2,3-*d*]pyrimidine antifolates with FRα and FRβ. For FRα, binding affinities were in the order, folic acid ∼ **7** ∼ **10** ∼ **11** ∼ **12** > **13** ≫ **9** ≫ MTX (Figure 3A). For the 6-pyrrolo[2,3-*d*]pyrimidines, these generally parallel relative levels of RT16 growth inhibition. For FRβ, binding affinities were in the order, folic acid > **10** ∼ **7** > **11**∼ **12** ∼ **13** ≫ **9** ∼ MTX (Figure 3B). Thus, the antiproliferative activities of the pyrrolopyrimidine analogues toward FRβ-expressing D4 cells were only partly reflected in their FR-binding affinities. Substantially reduced growth inhibition and FR α and β binding was seen for compound **9**. Whereas compounds **10**, **12**, and **13** bound avidly to FRα, accompanying loss of cell proliferation, for D4 cells, these poorly active analogues nonetheless showed detectable binding to FRβ, although binding was somewhat reduced for compounds **11**, **12**, and **13**. The decreased binding affinity for FRα and FRβ with **9**, accompanying loss of the terminal glutamate is analogous to previous findings of nonglutamyl nonbenzoyl 6-substituted pyrrolo[2,3-*d*]pyrimidine analogues.[15]

Additional experiments were performed to assess inhibitory effects of the amino acid analogues of **7** on PCFT membrane transport at pH 5.5 (the pH optimum for PCFT[24]), and at pH 6.8 (approximating the pH of the tumor microenvironment[25]), as a measure of relative binding affinities to the carrier (Figure 4). In these experiments, R2/PCFT4 CHO cells expressing human PCFT were incubated with [^{3}H]MTX (0.5 μM) in the presence of 1 or 10 μM of compounds **7** and **9**−**13** at 37 °C for 5 min. The antifolate PT523,[26] which is an excellent substrate for RFC transport but not for PCFT, was the negative control. At pH 5.5 and pH 6.8, **7** (10 μM) potently inhibited [^{3}H]MTX uptake (∼95% and ∼70%, respectively) (Figure 4); decreased inhibition (∼80% and ∼20% inhibition, at pH 5.5 and 6.8, respectively) was seen at 1 μM of compound **7**. Notably, 10 μM of compounds **11** and **13** also inhibited [^{3}H]MTX uptake by PCFT (∼75% and ∼70% inhibition, respectively, at pH 5.5, and ∼30% inhibition, each at pH 6.8) (Figure 4), even though these compounds did not inhibit proliferation of R2/PCFT4 cells (Table 1). Significant albeit reduced inhibition was measured at 1 μM for compounds **11** and **13** (10% and 25%, respectively, at pH 5.5). For compounds **11** and **13**, we calculated K_i values from Dixon analysis at pH 5.5 as measures of binding affinities for PCFT for comparison to **7**. By this analysis, K_is for **11** and **13** were 1.60 (±0.21) and 2.90 (±0.53) μM, whereas the calculated K_i value for compound **7** was 0.33 (±0.04) μM. Thus, **11** and **13** bind to PCFT, even though they are poorly

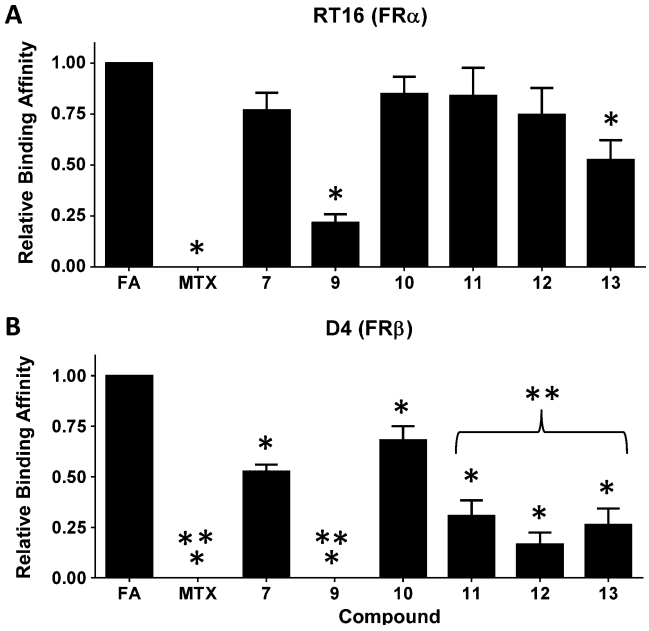

Figure 3. (A) Binding of 6-substituted pyrrolo[2,3-*d*]pyrimidine analogues (**9**−**13**) to FRα in RT16 cells and (B) FRβ in D4 compared to compound **7** and folic acid. Data are shown for the effects of the various ligands with FRα-expressing RT16 and FRβ-expressing D4 CHO cells. Relative binding affinities for assorted folate/antifolate substrates were determined over a range of ligand concentrations and were calculated as the inverse molar ratios of unlabeled ligands required to inhibit [^{3}H]folic acid binding by 50%. By definition, the relative affinity of folic acid is 1. Procedural details for the binding assays are provided in the Experimental Section. Results are presented as mean values ± standard errors from three experiments. Undefined abbreviations: FA, folic acid. For MTX and compounds **9** and **13** with FRα, and MTX and compounds **7**, **9**, **10**, **11**, **12**, and **13** with FRβ, differences in relative binding affinities were statistically significant from that for folic acid (noted with *; $p < 0.05$) by paired *t*-test analysis. For MTX and compounds **9**, **11**, **12**, and **13**, differences in relative binding affinities to FRβ were significantly different from that measured for compound **10** (noted with **; $p < 0.05$) by paired *t* test analysis.

dx.doi.org/10.1021/jm501113m | J. Med. Chem. 2014, 57, 8152−8166

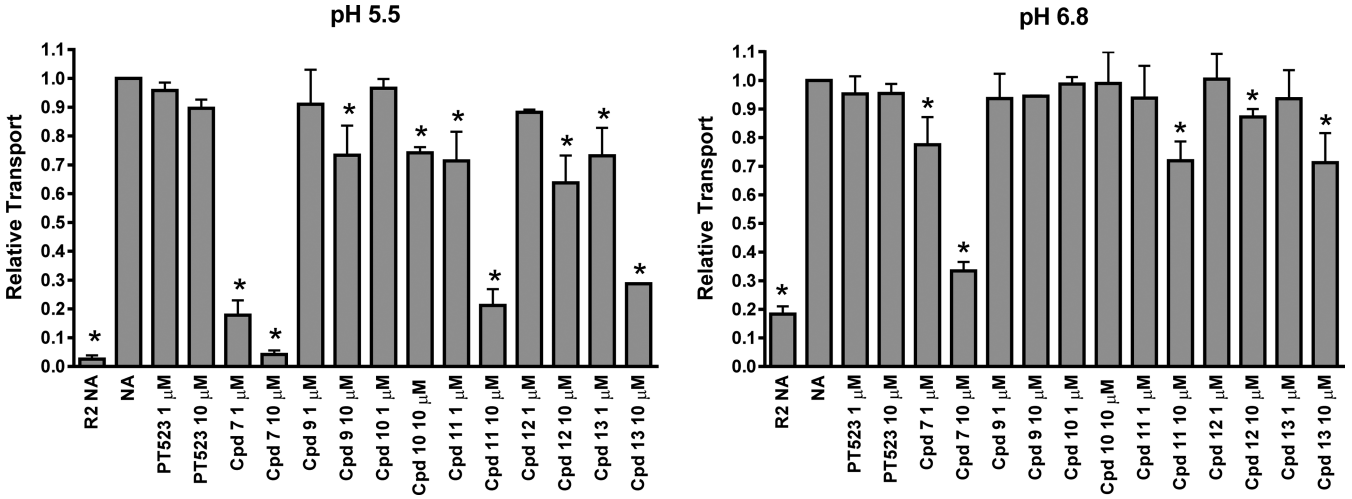

Figure 4. Binding of 6-substituted pyrrolo[2,3-*d*]pyrimidine analogues (**9**–**13**) to PCFT in R2/PCFT4, compared to **7**. Data are shown for the effects of the unlabeled ligands with R2/PCFT4 CHO cells. Relative PCFT binding affinities for assorted antifolate substrates were measured at pH 5.5 and pH 6.8 over 5 min in the presence [^{3}H]MTX (0.5 μM), with 1 or 10 μM of inhibitor. Experimental details are provided in the Experimental Section. Results are presented as mean values plus/minus standard errors for three experiments. Results are compared to normalized rates in the absence of any additions or in the presence of the RFC-selective inhibitor PT523,[26] and to PCFT-null R2 cells without additions. Undefined abbreviations: FA, folic acid; NA, no additions. The bars noted with asterisks were statistically different from the untreated control (NA) ($p < 0.05$) by paired *t*-test analysis.

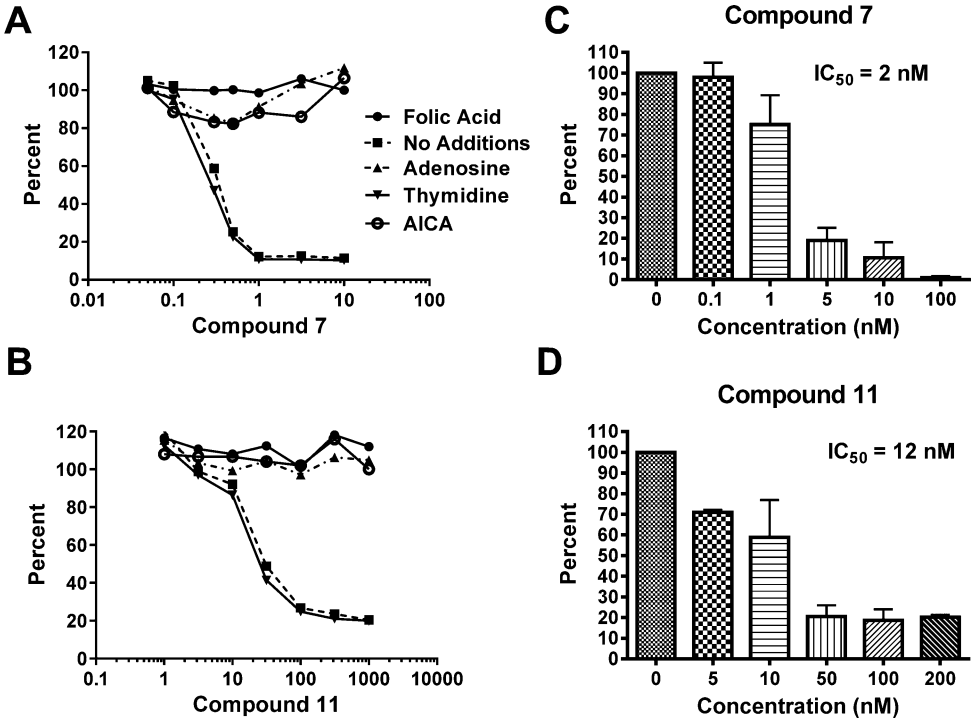

Figure 5. Compound **7** inhibits de novo purine nucleotide biosynthesis and GARFTase. (A,B) Results are shown for nucleoside/AICA protection experiments with KB cells over a range of concentrations of compounds **7** (A) and **11** (B). Experiments were performed in complete folate-free RPMI 1640 with 2 nM LCV in the absence of any additions (labeled "No additions"), or in the presence of 200 nM folic acid, adenosine (60 μM), thymidine (10 μM), or AICA (320 μM). Cell densities were measured with CellTiter Blue dye and a fluorescence plate reader. Results were normalized to cell densities in the absence of drug. Results shown are representative data from experiments performed in triplicate. (C,D) For the in situ GARFTase activity assays, incorporation of [^{14}C]glycine into [^{14}C]formyl GAR was measured in KB human tumor cells cultured for 15 h in complete folate-free RPMI 1640 plus 2 nM LCV. Experimental details are described in the Experimental Section. Results are presented as a percent of controls treated without drugs for KB cells treated with nM concentrations of **7** or **11**. Calculated IC_{50} values for GARFTase inhibition with compounds **7** and **11** are indicated.

internalized by this mechanism (as reflected in their inability to inhibit proliferation of R2/PCFT4 cells; Table 1).

GARFTase in de Novo Purine Nucleotide Biosynthesis Is the Major Intracellular Target for Compound 11 in KB Human Tumor Cells.

Compounds **10**, **11**, **12**, and **13** all inhibited proliferation of human FRα-expressing CHO RT16 cells. However, with human tumor KB cells which also express high levels of FRα,[13,19] compound **11** was singularly active

dx.doi.org/10.1021/jm501113m | J. Med. Chem. 2014, 57, 8152–8166

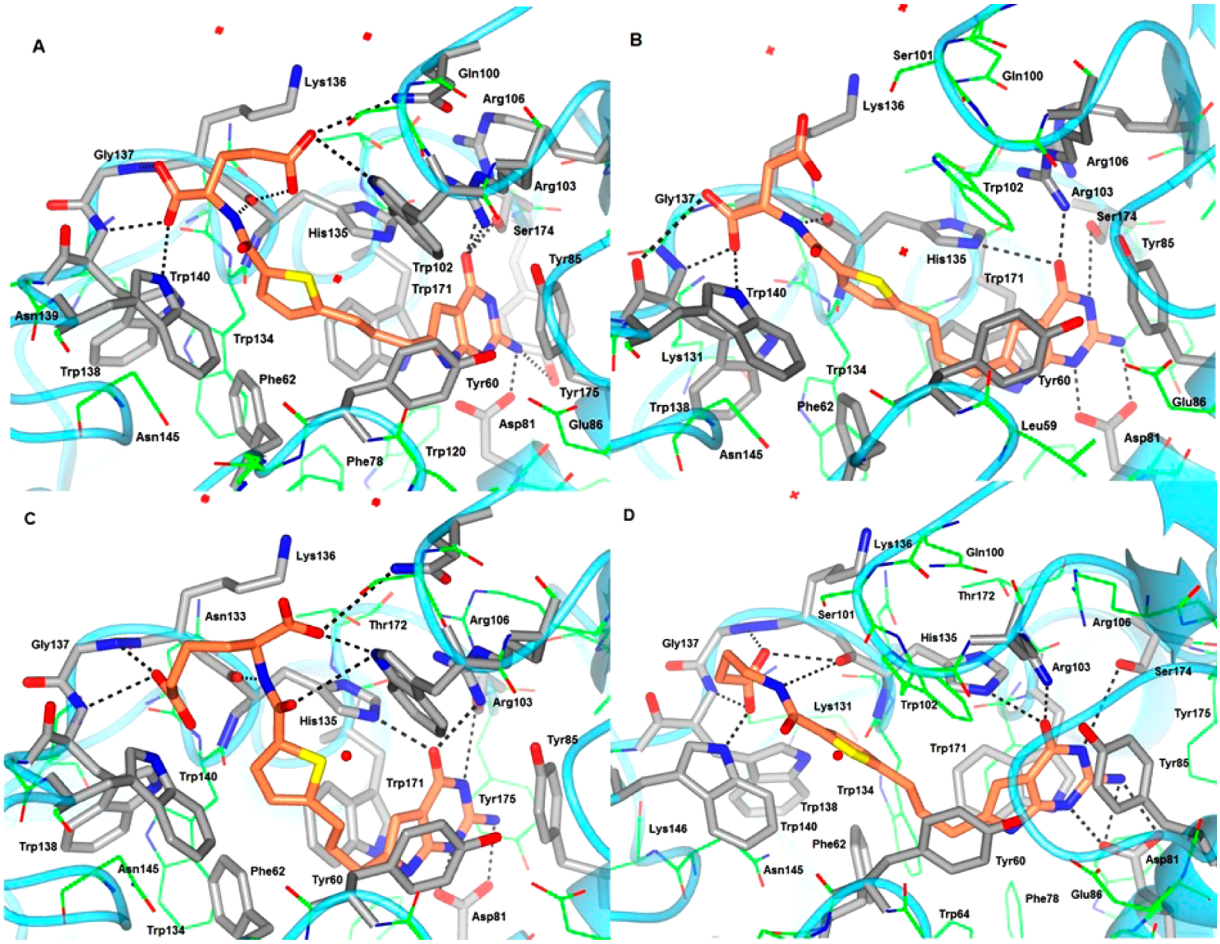

Figure 6. Molecular modeling studies of compounds **7** and **10**–**12** with FRα. (A) Docked pose of **7** (pink) in human FRα (PDB 4LRH).[27] Interacting amino acids in the binding pocket are depicted as gray cylinders (labeled), while noninteracting amino acids in the binding pocket are depicted as green lines (unlabeled). (B) Docked pose of **10** (pink) in human FRα (PDB 4LRH).[27] Interacting amino acids in the binding pocket are depicted as gray cylinders (labeled), while noninteracting amino acids in the binding pocket are depicted as green lines (unlabeled). (C) Docked pose of **11** (pink) in human FRα (PDB 4LRH).[27] Interacting amino acids in the binding pocket are depicted as gray cylinders (labeled), while noninteracting amino acids in the binding pocket are depicted as green lines (unlabeled). (D) Docked pose of **12** (pink) in human FRα (PDB 4LRH).[27] Interacting amino acids in the binding pocket are depicted as gray cylinders (labeled), while noninteracting amino acids in the binding pocket are depicted as green lines (unlabeled).

(Table 1). This suggests that there are substantial differences in metabolism or intracellular targeting of this series of compounds between human (KB) and hamster (RT16) cells, as previously described for another series of antifolate analogues.[23]

GARFTase is an established target for **7**, resulting in depletion of ATP pools.[18] To assess the possibility that the adipic acid analogue of **7**, compound **11**, also inhibited de novo purine nucleotide biosynthesis, we tested the capacity of exogenous adenosine (60 μM) to reverse its growth inhibition toward KB cells.[13,16−18,23] Results were compared to those for exogenous thymidine (10 μM). 5-Aminoimidazole-4-carboxamide (AICA) (320 μM), a precursor of the second folate-dependent step catalyzed by AICA ribonucleotide formyltransferase (AICARFTase), was also tested so as to distinguish inhibition of GARFTase from AICARFTase.[13,16−18,23] Thymidine had no effect on the inhibition of KB cell proliferation by **7** or **11**; however, both adenosine and AICA abolished the inhibitory effects (Figure 5A,B). These results establish that compound **11** like **7** is a potent inhibitor of de novo purine nucleotide biosynthesis, most likely at GARFTase.

To directly measure GARFTase activity in KB cells treated with **7** and **11**, we used an in situ GARFTase assay.[9,11−13,17] KB cells were incubated with [^{14}C]glycine as a radiotracer for 15 h in the presence of **7** or **11** under conditions and at concentrations approximating those used in the cell proliferation experiments (Table 1). In this assay, [^{14}C]glycine is incorporated into the GARFTase substrate [^{14}C]GAR and metabolized to [^{14}C]formyl GAR by GARFTase which accumulates in the presence of azaserine. [^{14}C]Formyl GAR is isolated by ion-exchange chromatography, quantified and levels normalized to cellular protein. Compound **11** is a GARFTase inhibitor in KB cells, albeit ~6-fold less potent than **7** (Figure 5C,D), paralleling the differences in antiproliferative activities (Table 1).

Molecular Modeling Studies. The X-ray crystal structures of human FRα[27] and FRβ[28] were recently published. In addition, the X-ray crystal structure of human GARFTase[29] is also known. Thus, it was of interest to dock our 6-substituted pyrrolo[2,3-*d*]pyrimidine analogues **7** and **9**–**13** into each of the known structures for FRα, FRβ, and GARFTase, to attempt to provide a molecular explanation for the biological activities

dx.doi.org/10.1021/jm501113m | *J. Med. Chem.* 2014, 57, 8152−8166

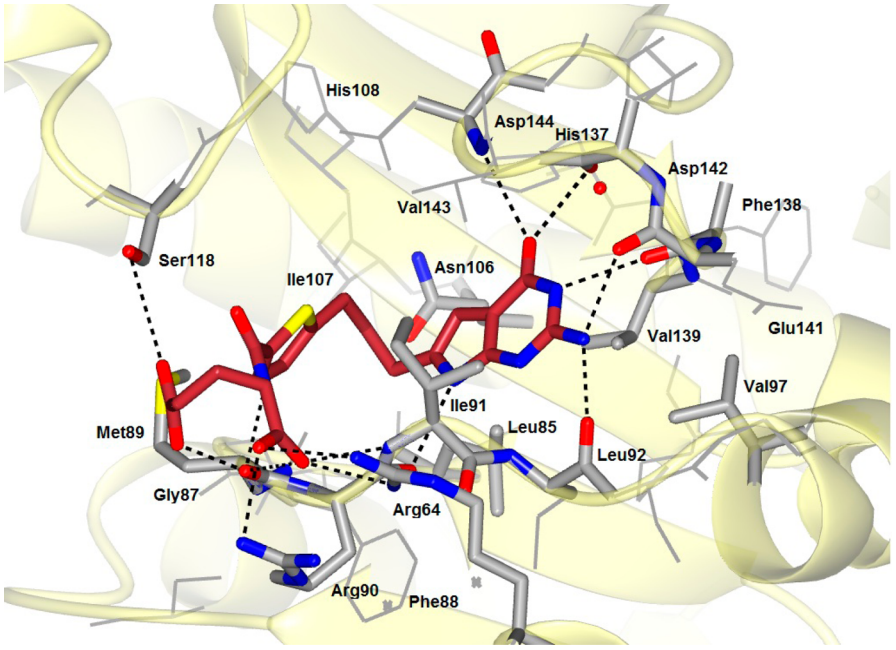

Figure 7. Molecular modeling of **7** with GARFTase. Docked pose of **7** (brown) in human GARFTase (PDB 1NJS).[29] Interacting amino acids in the binding pocket are depicted as gray cylinders (labeled), while noninteracting amino acids in the binding pocket are depicted as gray lines (unlabeled).

as well as the rank order of activities of the analogues for uptake by FRs and for GARFTase inhibition.

Figure 6A shows the docked pose of **7** in the human FRα (PDB 4LRH)[27] binding site. Compound **7** binds in the folate binding cleft of FRα. The 2-NH_2 and 4-oxo moieties of **7** interact with the same amino acids as the corresponding groups of folic acid,[27] with the 2-NH_2 interacting with Asp81 and the 4-oxo forming hydrogen bonds with the side chain hydroxyl of Ser174 and the side chain NH of Arg103. The pyrrolo[2,3-*d*]pyrimidine scaffold is sandwiched between the side chains of Tyr60 and Trp171, similar to that seen with the pteroyl ring of folic acid in its bound conformation. The L-glutamate moiety of **7** is oriented similarly to the corresponding glutamate in folic acid.[27] The α-carboxylic acid of **7** forms a network of hydrogen bonds involving the backbone NH of Gly137 (not labeled) and Trp138 and the side chain NH of Trp140. The γ-carboxylic acid interacts with the side chain NH groups of Gln100, Lys136, and Trp102 (not labeled), as is seen with the corresponding glutamate portion of folic acid in the crystal structure.[27] The thiophene ring of **7** forms hydrophobic interactions with Trp140. The hydrophobic 3-C linker of **7** forms nonspecific hydrophobic interactions with Tyr60, Phe62, Trp102, Trp134, and His135. The docking score of **7** was −40.35 kJ/mol, compared with that for folic acid of −44.67 kJ/mol.

The docked poses of **9**−**13** in human FRα retain the docking interactions of the pyrrolo[2,3-*d*]pyrimidine scaffold and the thienoyl side chain, as seen with the docked pose of **7** (Figure 6B−D shows docking results for compounds **10**−**13**). Variations in the docked orientation of the pteroic acid analogue **9** and the pentanoic acid analogue **13** from that of the glutamate chain of **7** could explain, in part, the differences observed in binding of these compounds to FRα (Figure 3). The loss of the terminal amino acid residue in **9** afforded docked poses (not shown) that retained the binding interactions of the pyrrolo[2,3-*d*]pyrimidine scaffold and the thienoyl carboxylic acid moieties but had significantly lower docking scores (−29.81 kJ/mol), as is reflected in its measured binding affinity for FRα (Figure 3). The α-COOH of the aspartate chain of **10** (Figure 6B) maintains the network of hydrogen bonds with Trp138 and Trp140 similar to that seen with the α-COOH of the glutamate chain of **7**. While the shorter chain length in the aspartic acid moiety of **10** prevents direct interaction of the γ-COOH with the binding pocket, it can be envisioned that water-mediated interactions of the γ-COOH with Lys136 and Trp102, as can be seen with the corresponding γ-COOH of **7**, could help in stabilizing the docked conformation. The docked score of **10** was −34.84 kJ/mol. In contrast, the adipic acid moiety in the docked conformation of **11** (Figure 6C) forms different interactions compared to the glutamate moiety in the docked conformation of **7**. The α-COOH in **11** interacts with Trp102 and Gln100, while the γ-COOH interacts with the side chains of Lys136 and Trp138. The docking score of **11** was −34.50 kJ/mol. The pentanoic acid moiety of **12** (Figure 6D) binds at the α-COOH binding site of **7** and interacts with the backbone NH of Lys136 and Trp138 and the side chain NH of Trp140. The docked score of this conformation was −33.64 kJ/mol. An alternate low-energy conformation of **12** (not shown), in which the terminal COOH mimics the γ-COOH of **7**, was observed in the docking study (docking score −31.02 kJ/mol). In contrast to **12**, the docked pose of **13** (not shown) showed the COOH group mimicking the α-COOH of **7**. The short chain length of **13** prevents binding to the γ-COOH binding site of **7** and could explain the reduced binding affinity of **13** against FRα (Figure 3). The docking score of **13** was −32.34 kJ/mol. Thus, the rank order of the docked scores of **7** and **9**−**13** for FRα parallel the growth inhibition results with FRα-expressing RT16 CHO cells (Table 1). Docking scores of **9**−**13** also parallel the relative binding affinities for FRα (Figure 3). However, for compound **7**, the docking score shows increased binding over

dx.doi.org/10.1021/jm501113m | *J. Med. Chem.* 2014, 57, 8152−8166

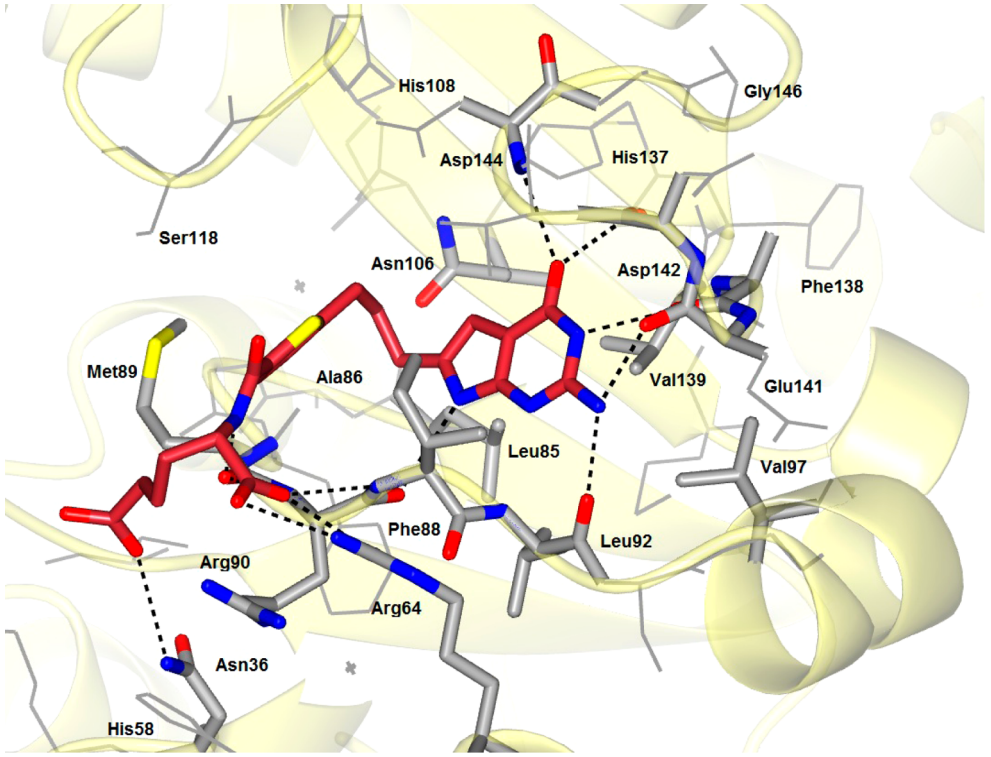

Figure 8. Molecular modeling of **11** with GARFTase. Docked pose of **11** (red) in human GARFTase (PDB 1NJS).[29] Interacting amino acids in the binding pocket are depicted as gray cylinders (labeled), while noninteracting amino acids in the binding pocket are depicted as gray lines (unlabeled).

analogues **10**−**12**, in contrast to the results of direct binding assays (Figure 3).

FRα and FRβ share 82% sequence identity and 92% sequence similarity.[28] The docked conformations of **9**−**13** in the X-ray crystal structure of FRβ bound to PMX (PDB 4KN2, not shown)[28] were very similar to those seen in the docking studies with FRα, described above. The docking studies with FRβ did not provide an adequate molecular explanation for the differences in binding affinities (rank order of binding), as measured by cell surface competition with [^{3}H]folic acid (Figure 3) or the biological activities of the analogues toward FRβ- compared to FRα-expressing CHO cells (Table 1), as described above.

Because compounds **7** and **11** were both shown to target GARFTase, it was of interest to dock **7** and **11** to explore the molecular basis of their activities against GARFTase. Thus, molecular modeling studies were carried out using the X-ray crystal structure of human GARFTase bound to trifluoroacetyl-5,10-dideaza-acyclic-5,6,7,8-tetrahydrofolic acid (10-CF_3CO-DDACTHF, PDB 1NJS).[29] Figure 7 shows the docked pose of **7** in the GARFTase active site. The pyrrolo[2,3-*d*]pyrimidine scaffold of **7** binds in the region occupied by the diaminopyrimidine ring in 10-CF_3CO-DDACTHF. This orientation of the scaffold permits interaction of the 2-NH_2 of **7** with the backbone of Leu92 and Asp141. The N3 nitrogen of **7** forms a hydrogen bond with the backbone of Ile140, while the 4-oxo moiety forms hydrogen bonds with the backbone atoms of Asp142 and Asp144. The pyrrole N7-nitrogen forms a hydrogen bond with the backbone of Arg90. The pyrrolo[2,3-*d*]pyrimidine scaffold of **7** forms hydrophobic interactions with Leu85, Ile91, Leu92, and Val97 and with the folate binding loop residues 141−146. The amide NH of the L-glutamate forms a hydrogen bond with Met89. The glutamate chain of **7** is oriented similar to the glutamate chain of 10-CF_3CO-DDACTHF with the α-COOH interacting with Arg64, Arg90, and the backbone of Ile91 and the γ-COOH interacting with the side chain hydroxyl of Ser116. The docking score of **7** in GARFTase was −54.33 kJ/mol.

Figure 8 shows the docked pose of **11** in the GARFTase active site. The docked pose is similar to that of **7** in GARFTase, described above. However, in **11**, the γ-COOH of the longer adipic acid moiety can form a hydrogen bond with Asn106. In addition, the carbon side chain of the adipic acid moiety can form van der Waal's interactions with the side chain carbon atoms of Met89 and Arg90. The docking score of **11** in GARFTase was −52.44 kJ/mol. These interactions of **7** and **11** explain the binding and rank order of potent inhibition of GARFTase, as demonstrated by the in situ GARFTase assays (Figure 5) of **7** and **11**.

With the recent report of the X-ray crystal structures of FRα[27] and FRβ,[28] it was of interest to determine the difference, if any, in the docked conformations of the side chains of our amino acid analogues for transport (FRα) and enzyme inhibition (GARFTase). On the basis of docking studies in FRα and GARFTase, it is apparent that the side chain thienoyl amino acid (e.g., glutamic acid (**7**), aspartic acid (**10**), adipic acid (**11**)) of the antifolate has a completely different orientation for FRα versus GARFTase with respect to the bicyclic pyrrolo[2,3-*d*]pyrimidine scaffold. Thus, a degree of flexibility in the amino acid side chain appears to be essential to provide both selective transport and potent enzyme inhibition.

CONCLUSIONS

This report continues studies to establish a comprehensive SAR for substrate binding and cellular uptake by the major clinically relevant (anti)folate uptake systems, RFC, PCFT, and FRα and

dx.doi.org/10.1021/jm501113m | J. Med. Chem. 2014, 57, 8152−8166

β. Uptake of novel cytotoxic antifolates by FRs or PCFT over RFC by tumor cells but not normal tissues would confer selectivity and result in decreased toxicity over standard antifolates such as MTX or PMX that are transported by all three uptake systems. We previously found that 6-substituted pyrrolo[2,3-*d*]pyrimidine thienoyl antifolates were excellent substrates for FRα and β and for PCFT, with poor substrate activities for RFC.[17,18,23] Compound **7**, the 3-carbon bridge analogue and the most potent of this series, was cytotoxic in vitro toward both FRα and PCFT-expressing cells, including clinically relevant human tumor cell lines.[18−20,30] In vivo efficacy was demonstrated toward both early and late stage human tumors in immune-compromised mice.[18,20,30] Antitumor effects were due to inhibition of GARFTase and ATP depletion.[18−20,30]

In this report, we explore the role of the terminal L-glutamate in compound **7** on FR and PCFT binding and cellular uptake. A series of 6-substitituted pyrrolo[2,3-*d*]pyrimidine thienoyl analogues based on **7** with replacements of L-glutamate by different amino acids was described. An additional analogue (**9**) with a terminal carboxyl and no amino acid moiety was also studied. Our results establish that amino acid modifications are well tolerated by FRα because none of the amino acid replacements completely abolished growth inhibition of FRα-expressing CHO cells. Deletion of the L-glutamate in **9** was particularly disruptive, but even for this analogue, a modest level of growth inhibition toward FRα-expressing CHO cells was detected. Conversely, different results were seen with FRβ, a close structural homologue of FRα, with only the adipic acid analogue of **7**, compound **11**, showing substantial antiproliferative activity toward D4 cells. For FRα-expressing CHO cells, the aspartate and adipate analogues, **10** and **11**, were the most potent of the series, with IC_{50}s nearly an order of magnitude higher than for **7**. Only **11** showed growth inhibitory activity toward KB tumor cells. For **11**, inhibition of GARFTase in KB cells was measured, analogous to compound **7** (albeit with a ∼ 6-fold decreased IC_{50}), results consistent with docking studies with human GARFTase.

While loss of inhibitory potency for compound **9** was reflected in substantially decreased binding affinity to FRα at the cell surface, for analogues **10**−**12**, there were comparatively modest differences in relative binding affinities that reasonably paralleled in vitro drug efficacies toward RT16 CHO cells engineered to express FRα. This rank order was also found in the docked scores of **9**−**13** in the crystal structure for FRα, although the docked score for compound **7** was disproportionate. The potent inhibition of FRα-expressing cells by compound **7**, compared to compounds **10**−**13**, likely reflects increased inhibition of GARFTase due to its efficient conversion to polyglutamates.[30] While the polyglutamylation of compounds **10**−**13** has not been tested, by analogy with 4-aminoantifolates with amino acid modifications (including aspartate and adipate analogues),[31,32] polyglutamylation of **10**−**13** is unlikely.

Although variations in surface binding affinities to FRβ in D4 cells among the assorted compounds were more pronounced than for FRα, with the exception of the undetectable binding for compound **9** and distinctly reduced binding affinities for compounds **12** and **13** for FRβ, these binding affinities could not explain the differences in in vitro efficacies toward FRα- versus FRβ-expressing CHO cells. Further, for most of the compounds, the docking studies could not explain the differences in relative binding affinities with FRα and FRβ.

Disparities between relative docking scores and binding affinities for FRα and β, or biological activities with FRα- or β-expressing cells, may reflect variations between the structures of soluble FRα and FRβ used for crystallization and the glycerol phosphatidylinositol-linked membrane-associated forms of FRα and FRβ used for the cell binding studies. The substantial differences in binding affinities for FRα and FRβ of **11**, **12**, and **13** (Figure 3), despite the high homology of the two transporters (see Supporting Information), may also reflect the differences in conformations of the two transporters when isolated and when bound to the membrane. These differences are not apparent in the (anti)folate binding sites in the X-ray crystal structures of FRα and β. For FRβ, the lack of agreement between the cell binding results and the in vitro proliferation assays may reflect differences in relative binding affinities of the bound substrates for FRβ at the cell surface and within the endosomes following internalization.

Whereas our results demonstrate that the terminal L-glutamate is not essential for binding and cellular uptake by FRs, there is an absolute requirement for L-glutamate for PCFT transport. Compound **7** is an excellent substrate for transport by PCFT essentially equivalent to PMX and with antiproliferative activity equaling or even exceeding that for PMX in engineered cell lines and human tumor cell line models.[18,20,30] None of the analogues of **7** with amino acid modifications that inhibited growth of RT16 CHO cells inhibited the isogenic PCFT-expressing R2/PCFT4 CHO cells, indicating that internalization of these analogues by PCFT was at best inefficient. However, both the adipic acid- (**11**) and the pentanoic acid-containing (**13**) analogues still competed with radiolabeled MTX in uptake assays at both pH 5.5 and 6.8 for PCFT, establishing binding to the carrier. For **13**, with only an α-carboxyl group, the greater inhibition of MTX transport over that seen with **12** suggested a greater importance of the α-carboxyl than the γ-carboxyl for substrate binding to human PCFT. These results raise the intriguing possibility that it may be possible to design agents that selectively block PCFT transport without internalization by this mechanism. If these agents do not compete for FR binding, they could be used in combination with FRα-targeted antifolates to augment FR-mediated cytotoxicity by competing with exogenous folate cofactors for transport by PCFT to reduce intracellular folate pools.[30] Studies are underway to explore this possibility.

In conclusion, this study provides structural evidence that the SAR for the major (anti)folate transporters (i.e., FRα, FRβ, PCFT, and RFC) for the pyrrolo[2,3-*d*]pyrimidine scaffold at the L-glutamate binding site are quite different. Thus, although **11** was less potent than **7**, it was more selective for FRα and FRβ over other cellular uptake processes. This characteristic may be used to afford increased selectivity for cellular uptake via FRs, depending on their expression in tumors vs normal cells, so as to provide targeted chemotherapy without dose-limiting toxicity.

EXPERIMENTAL SECTION

All evaporations were carried out in vacuo with a rotary evaporator. Analytical samples were dried in vacuo (0.2 mmHg) in a CHEM-DRY drying apparatus over P_2O_5 at 55 °C. Melting points were determined on a MEL-TEMP II melting point apparatus with a FLUKE 51 K/J electronic thermometer and are uncorrected. Nuclear magnetic resonance spectra for proton (^{1}H NMR) were recorded on a Bruker 400 MHz/52 MM (400 MHz) spectrometer. The chemical shift values are expressed in ppm (parts per million) relative to tetramethylsilane as internal standard: s, singlet: d, doublet; t, triplet; q, quartet; m,

dx.doi.org/10.1021/jm501113m | J. Med. Chem. 2014, 57, 8152−8166

mutiplet; br, broad singlet. The relative integrals of peak areas agreed with those expected for the assigned structures. High-resolution mass spectra (HRMS), using electron impact (EI), were recorded on a VG AUTOSPEC (Fisons Instruments) micromass (EBE Geometry) double focusing mass spectrometer. Thin-layer chromatography (TLC) was performed on Whatman Sil G/UV254 silica gel plates with fluorescent indicator, and the spots were visualized under 254 and 366 nm illumination. Proportions of solvents used for TLC are by volume. Column chromatography was performed on a 230−400 mesh silica gel (Fisher, Somerville, NJ) column. Elemental analyses were performed by Atlantic Microlab, Inc. Norcross, GA. Element compositions were within ±0.4% of the calculated values. Fractional moles of water or organic solvents found in some analytical samples could not be prevented despite 24−48 h of drying in vacuo and were confirmed where possible by their presence in the ^{1}H NMR spectra. All solvents and chemicals were purchased from Aldrich Chemical Co. or Fisher Scientific and were used as received. Purities of the final compounds **7**, **9**−**13** were >95% by elemental analysis.

5-(4-Hydroxy-but-1-ynyl)-thiophene-2-carboxylic Acid Methyl Ester (16). This compound was synthesized in 70% yield as described previously.[17] TLC R_f 0.33 (hexane/EtOAc 1:1). ^{1}H NMR (DMSO-d_6): δ 2.61 (t, J = 6.4 Hz, 2H, CH_2), 3.57 (t, J = 6.4 Hz, 2H, CH_2), 3.81 (s, 3H, $COOCH_3$), 4.96 (t, J = 5.6 Hz, 1H, OH, exch), 7.28 (d, J = 4.0 Hz, 1H, Ar), 7.70 (d, J = 4.0 Hz, 1H, Ar).

5-(4-Hydroxy-butyl)-thiophene-2-carboxylic Acid Methyl Ester (17). This compound was synthesized in 95% yield as described previously.[17] TLC R_f 0.34 (hexane/EtOAc 1:1). ^{1}H NMR (DMSO-d_6): δ 1.45 (m, 2H, CH_2), 1.64 (m, 2H, CH_2), 2.83 (t, J = 7.2 Hz, 2H, CH_2), 3.40 (m, 2H, CH_2), 3.77 (s, 3H, $COOCH_3$), 4.42 (t, J = 5.2 Hz, 1H, OH, exch), 6.95 (d, J = 3.6 Hz, 1H, Ar), 7.64 (d, J = 3.6 Hz, 1H, Ar).

5-(3-Carboxy-propyl)-thiophene-2-carboxylic Acid Methyl Ester (18). To acetonitrile (35 mL) was added H_5IO_6 (3.20 g, 14.05 mmol), and the mixture was stirred vigorously at room temperature for 15 min. Alcohol **17** (1.14 g, 5.30 mmol) was added to a cold solution (ice bath) of H_5IO_6 in acetonitrile. A solution of pyridinium chlorochromate (27.58 mg, 0.13 mmol) in acetonitrile (2 × 5 mL) was then added to the reaction mixture in two portions and allowed to stir for 3 h. The reaction mixture was then diluted with ethyl acetate (80 mL) and washed with brine water (1:1), satd aq $NaHSO_3$ solution, and brine, respectively, dried over anhyd Na_2SO_4, and concentrated to give pure carboxylic acid **18** (73%) as a colorless oil. TLC R_f 0.58 (hexane/EtOAc 1:1). ^{1}H NMR (DMSO-d_6): δ 1.84 (m, 2H, CH_2), 2.25 (t, J = 7.2 Hz, 2H, CH_2), 2.84 (t, J = 7.2 Hz, 2H, CH_2), 3.77 (s, 3H, $COOCH_3$), 6.96 (d, J = 3.6 Hz, 1H, Ar), 7.64 (d, J = 3.6 Hz, 1H, Ar), 12.17 (br, 1H, COOH, exch). HRMS calcd for $C_{10}H_{12}O_4S$ (M^+), 228.0456; found, 228.0458.

5-(5-Bromo-4-oxo-pentyl)-thiophene-2-carboxylic Acid Methyl Ester (21). Compound **21** was synthesized in 76% yield from **18** as described previously.[17] TLC R_f 0.71 (hexane/EtOAc 1:1). ^{1}H NMR ($CDCl_3$-d): δ 2.05 (m, 2H, CH_2), 2.73(t, J = 7.2 Hz, 2H, CH_2), 2.89 (t, J = 7.2 Hz, 2H, CH_2), 3.87 (s, 3H, $COOCH_3$), 3.88 (s, 2H, CH_2Br), 6.81−6.82 (d, J = 3.6 Hz, 1H, Ar), 7.65 (d, J = 3.6 Hz, 1H, Ar). HRMS calcd for $C_{11}H_{13}BrO_3S$ (M^+), 303.9769; found, 303.9759.

5-[3-(2-Amino-4-oxo-4,7-dihydro-3*H*-pyrrolo[2,3-*d*]-pyrimidin-6-yl)-propyl]-thiophene-2-carboxylic Acid Methyl Ester (23). Compound **23** was synthesized in 38% yield from **21** as described previously.[17] TLC R_f 0.17 ($CHCl_3$/MeOH 10:1); mp 175−176 °C, ^{1}H NMR (DMSO-d_6): δ 1.94 (m, 2H, CH_2), 2.52 (t, J = 7.2 Hz, 2H, CH_2), 2.84 (t, J = 7.2 Hz, 2H, CH_2), 3.78 (s, 3H, $COOCH_3$), 5.89 (s, 1H, C5-CH), 5.96 (s, 2H, 2-NH_2, exch), 6.98 (d, J = 3.6 Hz, 1H, Ar), 7.65 (d, J = 3.6 Hz, 1H, Ar), 10.13 (s, 1H, 3-NH, exch), 10.82 (s, 1H, 7-NH, exch).

5-[3-(2-Amino-4-oxo-4,7-dihydro-3*H*-pyrrolo[2,3-*d*]-pyrimidin-6-yl)-propyl]-thiophene-2-carboxylic Acid (9). Compound **9** was synthesized in 89% yield from **23** as described previously;[17] mp 175−176 °C. ^{1}H NMR (DMSO-d_6): δ 1.93 (m, 2H, CH_2), 2.52 (t, J = 7.2 Hz, 2H, CH_2), 2.82 (t, J = 7.2 Hz, 2H, CH_2), 5.88 (s, 1H, C5-CH), 5.98 (s, 2H, 2-NH_2, exch), 6.93 (d, J = 3.6 Hz, 1H, Ar), 7.56 (d, J = 3.6 Hz, 1H, Ar), 10.14 (s, 1H, 3-NH, exch), 10.83 (s, 1H, 7-NH, exch) 12.86 (br, 1H, COOH, exch). Anal. ($C_{14}H_{14}N_4O_3S$·0.25H_2O·0.2CH_3COOH) C, H, N, S.

(*S*)-2-({5-[3-(2-Amino-4-oxo-4,7-dihydro-3*H*-pyrrolo[2,3-*d*]-pyrimidin-6-yl)-propyl]-thiophene-2-carbonyl}-amino)-pentanedioic Acid (7). Compound **7** was synthesized from **9** in 56% yield as reported previously;[17] mp 168−169 °C. ^{1}H NMR (DMSO-d_6): δ 1.99 (m, 4H, β-CH_2, CH_2), 2.32 (t, J = 7.6 Hz, 2H, γ-CH_2), 2.52 (t, J = 7.2 Hz, 2H, CH_2), 2.80 (t, J = 7.2 Hz, 2H, CH_2), 4.33 (m, 1H, α-CH), 5.88 (s, 1H, C5-CH), 5.97 (s, 2H, 2-NH_2, exch), 6.90 (d, J = 3.6 Hz, 1H, Ar), 7.69 (d, J = 3.6 Hz, 1H, Ar), 8.51 (d, J = 8 Hz, 1H, CONH, exch), 10.13 (s, 1H, 3-NH, exch), 10.82 (s, 1H, 7-NH, exch) 12.42 (br, 2H, COOH, exch). Anal. ($C_{19}H_{21}N_5O_6S$·1.0H_2O): C, H, N, S.

(*S*)-2-({5-[3-(2-Amino-4-oxo-4,7-dihydro-3*H*-pyrrolo[2,3-*d*]-pyrimidin-6-yl)-propyl]-thiophene-2-carbonyl}-amino)-butanedioic Acid (10). To a solution of **9** (130 mg, 0.41 mmol) in anhydrous DMF (10 mL) was added *N*-methylmorpholine (84 mg, 0.72 mmol) and 2-chloro-4,6-dimethoxy-1,3,5-triazine (127 mg, 0.72 mmol). The resulting mixture was stirred at room temperature for 2 h. To this mixture were added *N*-methylmorpholine (84 mg, 0.72 mmol) and L-aspartic acid dimethyl ester hydrochloride (119 mg, 0.60 mmol). The reaction mixture was stirred for an additional 12 h at room temperature and then evaporated to dryness under reduced pressure. The residue was dissolved in the minimum amount of $CHCl_3$/MeOH (4:1) and chromatographed on a silica gel column (2 cm × 15 cm) and with 5% $CHCl_3$ in MeOH as the eluent. Fractions that showed the desired spot (TLC R_f 0.44 $CHCl_3$/MeOH 5:1) was pooled and the solvent evaporated to dryness to afford 122 mg (65%) of dimethylester as yellow powder. To a solution of dimethylester (122 mg, 0.26 mmol) in MeOH (5 mL) was added 1 N NaOH (10 mL), and the mixture was stirred under N_2 at room temperature for 16 h. TLC showed the disappearance of the starting material (R_f 0.44) and one major spot at the origin ($CHCl_3$/MeOH 5:1). The reaction mixture was evaporated to dryness under reduced pressure. The residue was dissolved in water (10 mL), the resulting solution was cooled in an ice bath, and the pH was adjusted to 3−4 with dropwise addition of 1 N HCl and then acetic acid. The resulting suspension was frozen in a dry ice−acetone bath, thawed to 4−5 °C in the refrigerator, and filtered. The residue was washed with a small amount of cold water and acetone. The residue was then dried in vacuum using P_2O_5 to afford 68 mg (59%) of **10** as white powder. Overall yield was 38% in two steps; mp 171−172 °C. ^{1}H NMR (DMSO-d_6): δ 1.93 (m, 2H, CH_2), 2.53 (m, 2H, CH_2), 2.73 (m, 4H, β-CH_2 and CH_2), 4.67 (m, 1H, α-CH), 5.90 (d, 1H, C5-CH), 5.98 (s, 2H, NH_2), 6.90 (d, 1H, J = 3.2 Hz, Ar), 7.62 (d, 1H, J = 3.2 Hz, Ar), 8.65 (d, 1H, J = 8 Hz, CONH, exch), 10.15 (s, 1H, 3-NH, exch), 10.84 (s, 1H, 7-NH, exch), 12.60 (br, 2H, COOH, exch). Anal. ($C_{18}H_{19}N_5O_6S$·0.25CH_3COCH_3·1CH_3COOH) C, H, N, S.

(*S*)-2-({5-[3-(2-Amino-4-oxo-4,7-dihydro-3*H*-pyrrolo[2,3-*d*]-pyrimidin-6-yl)propyl]thiophene-2-carbonyl}-amino)-hexanedioic Acid (11). To a solution of **9** (150 mg, 0.47 mmol) in anhydrous DMF (10 mL) was added *N*-methylmorpholine (99 mg, 0.85 mmol) and 2-chloro-4,6-dimethoxy-1,3,5-triazine (150 mg, 0.85 mmol). The resulting mixture was stirred at room temperature for 2 h. To this mixture were added *N*-methylmorpholine (150 mg, 0.47 mmol) and dimethyl (*S*)-2-aminohexanedioate (134 mg, 0.71 mmol). The reaction mixture was stirred for an additional 12 h at room temperature and then evaporated to dryness under reduced pressure. The residue was dissolved in the minimum amount of $CHCl_3$/MeOH (4:1) and chromatographed on a silica gel column (2 cm × 15 cm) and with 5% $CHCl_3$ in MeOH as the eluent. Fractions that showed the desired spot (TLC R_f 0.46 $CHCl_3$/MeOH 5:1) were pooled and the solvent evaporated to dryness to afford 152 mg (66%) of dimethylester as yellow powder. To a solution of dimethylester (152 mg, 0.31 mmol) in MeOH (5 mL) was added 1 N NaOH (10 mL), and the mixture was stirred under N_2 at room temperature for 16 h. TLC showed the disappearance of the starting material (R_f 0.46) and one major spot at the origin ($CHCl_3$/MeOH 5:1). The reaction mixture was evaporated to dryness under reduced pressure. The residue was dissolved in water (10 mL), the resulting solution was cooled in an ice bath, and the pH was adjusted to 3−4 with dropwise addition of 1 N HCl and then

dx.doi.org/10.1021/jm501113m | J. Med. Chem. 2014, 57, 8152−8166

acetic acid. The resulting suspension was frozen in a dry ice−acetone bath, thawed to 4−5 °C in the refrigerator, and filtered. The residue was washed with a small amount of cold water and acetone. The residue was then dried in vacuum using P_2O_5 to afford 116 mg (81%) of **11** as white powder. Overall yield was 53% in two steps; mp 165−167 °C. ^{1}H NMR (DMSO-d_6): δ 1.58 (m, 2H, CH_2), 1.77 (m, 2H, CH_2), 1.93 (t, J = 7 Hz, 2H, CH_2), 2.23 (t, J = 7 Hz, 2H, CH_2), 2.52 (t, J = 7 Hz, 2H, CH_2), 2.81 (t, J = 7 Hz, 2H, CH_2), 4.30 (m, 1H, α-CH), 5.90 (s, 1H, C5-CH), 5.97 (s, 2H, 2-NH_2, exch), 6.90 (d, J = 3.5 Hz, 1H, Ar), 7.72 (d, J = 3.5 Hz, 1H, Ar), 8.50 (d, J = 8 Hz, 1H, CONH, exch), 10.14 (s, 1H, 3-NH, exch), 10.83 (s, 1H, 7-NH, exch) 12.42 (br, 2H, COOH, exch). Anal. ($C_{20}H_{23}N_5O_6S\cdot1.25H_2O$) C, H, N, S.

4-({5-[3-(2-Amino-4-oxo-4,7-dihydro-3*H*-pyrrolo[2,3-*d*]-pyrimidin-6-yl)propyl]thiophene-2-carbonyl}-amino)-butanoic Acid (12). To a solution of **9** (254 mg, 0.80 mmol) in anhydrous DMF (10 mL) was added *N*-methylmorpholine (145 mg, 1.44 mmol) and 2-chloro-4,6-dimethoxy-1,3,5-triazine (253 mg, 1.44 mmol). The resulting mixture was stirred at room temperature for 2 h. To this mixture were added *N*-methylmorpholine (145 mg, 1.44 mmol) and methyl 4-aminobutyrate hydrochloride (193 mg, 1.26 mmol). The reaction mixture was stirred for an additional 12 h at room temperature and then evaporated to dryness under reduced pressure. The residue was dissolved in the minimum amount of $CHCl_3$/MeOH (4:1) and chromatographed on a silica gel column (2 cm × 15 cm) and with 5% $CHCl_3$ in MeOH as the eluent. Fractions that showed the desired spot (TLC R_f 0.58 $CHCl_3$/MeOH 5:1) were pooled and the solvent evaporated to dryness to afford 252 mg (76%) of methylester as yellow powder. To a solution of methylester (252 mg, 0.60 mmol) in MeOH (5 mL) was added 1 N NaOH (10 mL), and the mixture was stirred under N_2 at room temperature for 16 h. TLC showed the disappearance of the starting material (R_f 0.58) and one major spot at the origin ($CHCl_3$/MeOH 5:1). The reaction mixture was evaporated to dryness under reduced pressure. The residue was dissolved in water (10 mL), the resulting solution was cooled in an ice bath, and the pH was adjusted to 3−4 with dropwise addition of 1 N HCl and then acetic acid. The resulting suspension was frozen in a dry ice−acetone bath, thawed to 4−5 °C in the refrigerator, and filtered. The residue was washed with a small amount of cold water and acetone. The residue was then dried in vacuum using P_2O_5 to afford 188 mg (77%) of **12** as white powder. Overall yield was 58% in two steps; mp 168−169 °C. ^{1}H NMR (DMSO-d_6): δ 1.71 (q, J = 7.2 Hz, 2H, CH_2), 1.92 (q, J = 7.6 Hz, 2H, CH_2), 2.26 (t, J = 7.2 Hz, 2H, CH_2), 2.53 (t, J = 7.6 Hz, 2H, CH_2), 2.79 (t, J = 7.6 Hz, 2H, CH_2), 3.22 (t, J = 6.8 Hz, 2H, CH_2), 5.90 (s, 1H, C5-CH), 5.98 (s, 2H, 2-NH_2, exch), 6.88 (d, J = 3.5 Hz, 1H, Ar), 7.57 (d, J = 3.5 Hz, 1H, Ar), 8.39 (t, J = 5.6 Hz, 1H, CONH, exch), 10.15 (s, 1H, 3-NH, exch), 10.84 (d, 1H, J = 1.8 Hz, 7-NH, exch) 12.86 (br, 1H, COOH, exch). Anal. ($C_{18}H_{21}N_5O_4S\cdot0.5H_2O\cdot0.25CH_3COOH$) C, H, N, S.

(*S*)-2-({5-[3-(2-Amino-4-oxo-4,7-dihydro-3*H*-pyrrolo[2,3-*d*]-pyrimidin-6-yl)propyl]thiophene-2-carbonyl}-amino)-pentanoic Acid (13). To a solution of **9** (150 mg, 0.47 mmol) in anhydrous DMF (10 mL) was added *N*-methylmorpholine (99 mg, 0.85 mmol) and 2-chloro-4,6-dimethoxy-1,3,5-triazine (150 mg, 0.85 mmol). The resulting mixture was stirred at room temperature for 2 h. To this mixture were added *N*-methylmorpholine (150 mg, 0.47 mmol) and (*S*)-methyl 2-aminopentanoate hydrochloride (119 mg, 0.71 mmol). The reaction mixture was stirred for an additional 12 h at room temperature and then evaporated to dryness under reduced pressure. The residue was dissolved in the minimum amount of $CHCl_3$/MeOH (4:1) and chromatographed on a silica gel column (2 cm × 15 cm) and with 5% $CHCl_3$ in MeOH as the eluent. Fractions that showed the desired spot (TLC R_f 0.60 $CHCl_3$/MeOH 5:1) was pooled and the solvent evaporated to dryness to afford 168 mg (83%) of methyl ester as yellow powder. To a solution of methyl ester (168 mg, 0.39 mmol) in MeOH (5 mL) was added 1 N NaOH (10 mL), and the mixture was stirred under N_2 at room temperature for 16 h. TLC showed the disappearance of the starting material (R_f 0.60) and one major spot at the origin ($CHCl_3$/MeOH 5:1). The reaction mixture was evaporated to dryness under reduced pressure. The residue was dissolved in water (10 mL), the resulting solution was cooled in an ice bath, and the pH was adjusted to 3−4 with dropwise addition of 1 N HCl and then acetic acid. The resulting suspension was frozen in a dry ice−acetone bath, thawed to 4−5 °C in the refrigerator, and filtered. The residue was washed with a small amount of cold water and acetone. The residue was then dried in vacuum using P_2O_5 to afford 139 mg (86%) of **13** as white powder. Overall yield was 70% in two steps; mp 163−165 °C. ^{1}H NMR (DMSO-d_6): δ 0.89 (t, J = 7.6 Hz, 2H, CH_2), 1.35 (m, 2H, CH_2), 1.74 (m, 2H, CH_2), 1.93 (t, J = 7 Hz, 2H, CH_2), 2.54 (t, J = 7.2 Hz, 2H, CH_2), 2.81 (t, J = 7.2 Hz, 2H, CH_2), 4.32 (m, 1H, α-CH), 5.92 (s, 1H, C5-CH), 6.10 (bs, 2H, 2-NH_2, exch), 6.91 (d, J = 3.5 Hz, 1H, Ar), 7.73 (d, J = 3.5 Hz, 1H, Ar), 8.49 (d, J = 8 Hz, 1H, CONH, exch), 10.28 (s, 1H, 3-NH, exch), 10.91 (s, 1H, 7-NH, exch) 12.42 (br, 1H, COOH, exch). Anal. ($C_{19}H_{23}N_5O_4S\cdot1H_2O\cdot0.5CH_3COOH$) C, H, N, S.

Molecular Modeling and Computational Studies. The X-ray crystal structures of human FRα bound to folic acid (PDB 4LRH, 2.80 Å),[27] of FRβ bound to PMX (PDB 4KN2, 2.60 Å)[28] and of human GARFTase bound to 10-CF_3CO-DDACTHF (PDB 1NJS, 1.98 Å)[29] were obtained from the Protein Data Bank.

Docking studies were performed using LeadIT 2.1.6.[33] The protonation state of the proteins and the ligands were calculated using the default settings. Water molecules in the active site were permitted to rotate freely. The active site was defined by a sphere of 6.5 Å from the native ligand in the crystal structure. Ligands for docking were prepared using MOE 2013.08,[34] and the energy was minimized using the MMF94X force field to a constant of 0.05 kcal/mol. Triangle matching was used as the placement method and the docked poses were scored using default settings. The docked poses were visualized using CCP4MG.[35]

Molecules used for the docking experiments were constructed in MOE 2013.08 and minimized using the MMFF94x force field to a constant of 0.05 kcal/mol. To validate LeadIT 2.1.6 for docking the proposed compounds, the ligands, folic acid for FRα, PMX for FRβ, and 10-CF_3CO-DDACTHF for GARFTase, were built using the molecule builder function in MOE, energy minimized, and docked, as described above. RMSD of the docked poses were calculated using an SVL code obtained from the MOE Web site (www.chemcomp.com) and compared to the conformation of the crystal structure ligands.

The best docked pose of folic acid in FRα had an RMSD of 0.81 Å, PMX in FRβ had an RMSD of 1.01 Å and 10-CF_3CO-DDACTHF in the human GARFTase had an RMSD of 1.04 Å. Thus, LeadIT 2.1.6 was validated for our docking purposes in FRα, FRβ, and GARFTase.

Reagents for Biological Studies. [3′,5′,7,9-^{3}H]Folic acid (25 Ci/mmol), [3′,5′,7-^{3}H]MTX (20 Ci/mmol), and [^{14}C(U)]glycine (87mCi/mmol) were purchased from Moravek Biochemicals (Brea, CA). Unlabeled folic acid was purchased from Sigma Chemical Co. (St. Louis, MO). Leucovorin [(6*R*,*S*)-5-formyl tetrahydrofolate] (LCV) was obtained from the Drug Development Branch, National Cancer Institute, Bethesda, MD. The sources of the classical antifolate drugs were as follows: MTX, Drug Development Branch, National Cancer Institute (Bethesda, MD); RTX [*N*-(5-[*N*-(3,4-dihydro-2-methyl-4-oxyquinazolin-6-ylmethyl)-*N*-methylamino]-2-thienoyl)-L-glutamic acid], AstraZeneca Pharmaceuticals (Maccesfield, Cheshire, England); and PMX [*N*-{4-[2-(2-amino-3,4-dihydro-4-oxo-7*H*-pyrrolo[2,3-*d*]pyrimidin-5-yl)ethyl]benzoyl}-L-glutamic acid] (Alimta), Eli Lilly and Co. (Indianapolis, IN). Other chemicals were obtained from commercial sources in the highest available purity.

Cell Lines and Assays of Antitumor Drug Activities. The origin of the engineered CHO sublines including RFC- and FRα-null MTXRIIOua^{R}2-4 (R2), and RFC- (PC43-10), PCFT- (R2/PCFT4), FRα- (RT16), and FRβ (D4)-expressing CHO sublines were previously described.[13,16,21,22] Likewise, pCDNA3.1 vector control CHO cells (R2/VC) were reported.[13] The CHO cells were cultured in α-minimal essential medium (MEM) supplemented with 10% bovine calf serum (Invitrogen, Carlsbad, CA), 100 units/mL penicillin/100 μg/mL streptomycin, and 2 mM L-glutamine at 37 °C with 5% CO_2. All the R2 transfected cells [PC43-10, RT16, R2/hPCFT4, R2(VC)] were cultured in α-MEM plus 1.5 mg/mL G418. Prior to the cell proliferation assays (see below), RT16 cells were cultured in complete

dx.doi.org/10.1021/jm501113m | J. Med. Chem. 2014, 57, 8152−8166

folate-free RPMI 1640 (without added folate) for 3 days. R2/hPCFT4 and R2(VC) cells were cultured in complete folate-free RPMI 1640 including dialyzed fetal bovine serum (FBS) (Invitrogen) and 25 nM LCV with 1.5 mg/mL G418. KB human nasopharyngeal carcinoma cells were purchased from the American Type Culture Collection (Manassas, VA). KB cells were routinely cultured in folate-free RPMI 1640 medium, supplemented with 10% FBS, penicillin−streptomycin solution, and 2 mM L-glutamine at 37 °C with 5% CO_2.

For growth inhibition assays, cells (CHO and KB) were plated in 96 well dishes (~2500−5000 cells/well, total volume of 200 μL medium) with a range of antifolate concentrations.[13,16] The medium was RPMI 1640 (contains 2.3 μM folic acid) with 10% dialyzed FBS and antibiotics for experiments with R2 and PC43-10 cells. For RT16, D4, and KB cells, cells were cultured in folate-free RPMI media with 10% dialyzed FBS and antibiotics supplemented with 2 nM LCV and 2 mM L-glutamine. The requirement for FR-mediated drug uptake in these assays was established in parallel incubations including 200 nM folic acid. For R2/hPCFT4 cells, the medium was folate-free RPMI 1640 (pH 7.2) containing 25 nM LCV, supplemented with 10% dialyzed FBS, antibiotics, and L-glutamine. Cells were incubated for up to 96 h, and viable cells were assayed with CellTiter-Blue cell viability assay (Promega, Madison, WI) using a fluorescence plate reader.[13,16] Raw data were exported from Softmax Pro software to an Excel spreadsheet for analysis and determinations of IC_{50}s, corresponding to the drug concentrations that result in 50% loss of cell growth.

For some of the in vitro growth inhibition studies, the inhibitory effects of the antifolate inhibitors on de novo thymidylate biosynthesis (i.e., thymidylate synthase) and de novo purine nucleotide biosynthesis (GARFTase and AICARFTase) were tested by coincubations with thymidine (10 μM) and adenosine (60 μM), respectively.[13,16−18,23] For de novo purine nucleotide biosynthesis, additional protection experiments used AICA (320 μM) to distinguish inhibitory effects at GARFTase from those at AICARFTase.[13,16−18,23]

FR Binding Assay. Competitive inhibition of [^{3}H]folic acid binding to FRα and FRβ using RT16 and D4 CHO cells, respectively, was used was used to assess relative binding affinities for assorted (anti)folate ligands.[13,16−18,23] Cells were plated in 60 mm culture dishes 48 h prior to experiment. For the experiments, cells (~5 × 10^6) were rinsed twice with Dulbecco's phosphate-buffered saline (DPBS), followed by two washes with an acidic buffer (10 mM sodium acetate, 150 mM NaCl, pH 3.5) to remove FR-bound folates. Cells were washed twice with ice-cold HEPES-buffered saline (20 mM HEPES, 140 mM NaCl, 5 mM KCl, 2 mM $MgCl_2$, 5 mM glucose, pH7.4) (HBS), then incubated in HBS with [^{3}H]folic acid (50 nM, specific activity 0.5 Ci/mmol) in the presence and absence of unlabeled folic acid or antifolate (over a range of concentrations) for 15 min at 0 °C. The dishes were rinsed three times with ice-cold HBS, after which the cells were solubilized (0.5 N NaOH) and aliquots measured for radioactivity and protein contents. Protein concentrations were measured with Folin phenol reagent.[36] [^{3}H]Folic acid bound to FRα and FRβ was calculated as pmol/mg protein, and relative binding affinities were calculated as the inverse molar ratios of unlabeled ligands required to inhibit [^{3}H]folic acid binding by 50%.[11,12,14−16] By definition, the relative affinity of folic acid was 1.

Transport Assays. R2 and R2/hPCFT4 CHO sublines were routinely grown in suspension as spinner cultures at densities of 2−5 × 10^5 cells/mL. Cells were collected by centrifugation and washed with DPBS, and the cell pellets (~2 × 10^7 cells) were suspended in transport buffer (2 mL) for cellular uptake assays. pH-dependent uptake of 0.5 μM [^{3}H]Mtx was assayed in cell suspensions over 2 min at 37 °C in HBS at pH 6.8 or in 4-morphilinopropane sulfonic (MES)-buffered saline (20 mM MES, 140 mM NaCl, 5 mM KCl, 2 mM $MgCl_2$, and 5 mM glucose) at pH 5.5 in the presence or 1 or 10 μM inhibitor.[14] At the end of the incubations, transport was quenched with ice-cold DPBS, cells were washed 3 times with ice-cold DPBS, and cellular proteins were solubilized with 0.5 N NaOH. Levels of drug uptake were expressed as pmol/mg protein, calculated from direct measurements of radioactivity and protein contents of cell homogenates. Radioactivity was measured with a scintillation counter, and proteins were quantified using Folin-phenol reagent.[36] Transport results were normalized to levels in untreated controls. For determining K_i values for compounds **7**, **11** and **13**, transport was measured over 2 min with 0.5 μM [^{3}H]MTX and 0−5 μM of the unlabeled antifolate. Data was analyzed by Dixon plots.

In Situ GARFT Enzyme Inhibition Assay. Incorporation of [^{14}C]glycine into [^{14}C]formyl GAR, as an in situ measure of endogenous GARFTase activity, was measured.[13,16,17,11−17] For these experiments, KB cells were seeded in 4 mL complete folate-free RPMI 1640 plus 2 nM LCV in 60 mm dishes at a density of 2 × 10^6 cells per dish. On the next day, the medium was replaced with 2 mL of fresh complete folate-free RPMI 1640 plus 2 nM LCV (without supplementing glutamine). Azaserine (4 μM final concentration) was added in the presence and absence of the antifolate inhibitors. After 30 min, L-glutamine (final concentration, 2 mM) and [^{14}C]glycine (tracer amounts; final specific activity 0.1 mCi/L) were added. Incubations were at 37 °C for 15 h, at which time cells were washed (one-time) with ice-cold folate-free RPMI 1640 plus serum. Cell pellets were dissolved in 2 mL of 5% trichloroacetic acid at 0 °C. Cell debris was removed by centrifugation (the cell protein contents in the pellets were measured following solubilization with 0.5 N NaOH[36]), and the supernatants were extracted twice with 2 mL of ice-cold ether. The aqueous layer was passed through a 1 cm column of AG1 × 8 (chloride form), 100−200 mesh (Bio-Rad), washed with 10 mL of 0.5N formic acid, and then 10 mL of 4N formic acid, and finally eluted with 8 mL 1 N HCl. The eluates were collected and determined for radioactivity. The accumulation of [^{14}C]formyl GAR was calculated as pmol per mg protein over a range of inhibitor concentrations. IC_{50}s were calculated as the concentrations of inhibitors that resulted in a 50% decrease in [^{14}C]formyl GAR synthesis.

■ ASSOCIATED CONTENT

Ⓢ Supporting Information

Elemental analysis and sequence alignment between human folate receptor α and folate receptor β. This material is available free of charge via the Internet at http://pubs.acs.org

■ AUTHOR INFORMATION

Corresponding Authors

*For A.G.: phone, 412-396-6070; fax, 412-396-5593; E-mail, gangjee@duq.edu.

*For L.H.M.: phone, 313-578-4280; fax, 313-578-4287; E-mail, matherly@karmanos.org.

Author Contributions

⊥These authors (L.H.M. and A.G.) contributed equally to this work.

Notes

The authors declare no competing financial interest.

■ ACKNOWLEDGMENTS

This work was supported in part by grants from the National Institutes of Health, National Cancer Institute CA152316 (L.H.M. and A.G.), CA166711 (A.G. and L.H.M.), and CA53535 (L.H.M.), and the Duquesne University Adrian Van Kaam Chair in Scholarly Excellence (A.G.). M. R. Wilson was supported by a predoctoral training grant (T32 CA009531) from the National Cancer Institute.

■ ABBREVIATIONS USED

AIC, 5-aminoimidazole-4-carboxamide; AICARFTase, 5-aminoimidazole-4-carboxamide ribonucleotide formyltransferase; CHO, Chinese hamster ovary; FBS, fetal bovine serum; DPBS, Dulbecco's phosphate-buffered saline; FR, folate receptor; GAR, glycinamide ribonucleotide; GARFTase, glycinamide ribonucleotide formyltransferase; HBSS, Hank's balanced salts solution; HBS, HEPES-buffered saline; IC_{50}, 50%

inhibitory concentration; LCV, leucovorin; MTX, methotrexate; MEM, minimal essential media; PMX, Pemetrexed; PCFT, proton-coupled folate transporter; RTX, raltiterxed; RFC, reduced folate carrier; SAR, structure−activity relationship

REFERENCES

(1) Elnakat, H.; Ratnam, M. Distribution, functionality and gene regulation of folate receptor isoforms: Implications in targeted therapy. *Adv. Drug Delivery Rev.* **2004**, *56*, 1067−1084.

(2) Matherly, L. H.; Hou, Z.; Deng, Y. Human reduced folate carrier: Translation of basic biology to cancer etiology and therapy. *Cancer Metastasis Rev.* **2007**, *26*, 111−128.

(3) Zhao, R.; Diop-Bove, N.; Visentin, M.; Goldman, I. D. Mechanisms of membrane transport of folates into cells and across epithelia. *Annu. Rev. Nutr.* **2011**, *31*, 177−201.

(4) Kugel Desmoulin, S.; Hou, Z.; Gangjee, A.; Matherly, L. H. The human proton-coupled folate transporter: Biology and therapeutic applications to cancer. *Cancer Biol. Ther.* **2012**, *13*, 1355−1373.

(5) Matherly, L. H.; Wilson, M. R.; Hou, Z. The major facilitative folate transporters solute carrier 19A1 and solute carrier 46A1: Biology and role in antifolate chemotherapy of cancer. *Drug Metab. Dispos.* **2014**, *42*, 632−649.

(6) Zhao, R.; Matherly, L. H.; Goldman, I. D. Membrane transporters and folate homeostasis: Intestinal absorption and transport into systemic compartments and tissues. *Expert Rev. Mol. Med.* **2009**, *11*, e4.

(7) Nunez, M. I.; Behrens, C.; Woods, D. M.; Lin, H.; Suraokar, M.; Kadara, H.; Hofstetter, W.; Kalhor, N.; Lee, J. J.; Franklin, W.; Stewart, D. J.; Wistuba, II. High expression of folate receptor alpha in lung cancer correlates with adenocarcinoma histology and EGFR [corrected] mutation. *J. Thorac. Oncol.* **2012**, *7*, 833−840.

(8) Visentin, M.; Zhao, R.; Goldman, I. D. The antifolates. *Hematol. Oncol. Clin. North Am.* **2012**, *26*, 629−648.

(9) Gonen, N.; Assaraf, Y. G. Antifolates in cancer therapy: Structure, activity and mechanisms of drug resistance. *Drug Resist. Update* **2012**, *15*, 183−210.

(10) Yang, J.; Vlashi, E.; Low, P. Folate-linked drugs for the treatment of cancer and inflammatory diseases. *Subcell. Biochem.* **2012**, *56*, 163−179.

(11) Reddy, J. A.; Dorton, R.; Westrick, E.; Dawson, A.; Smith, T.; Xu, L. C.; Vetzel, M.; Kleindl, P.; Vlahov, I. R.; Leamon, C. P. Preclinical evaluation of EC145, a folate-vinca alkaloid conjugate. *Cancer Res.* **2007**, *67*, 4434−4442.

(12) Naumann, R. W.; Coleman, R. L.; Burger, R. A.; Sausville, E. A.; Kutarska, E.; Ghamande, S. A.; Gabrail, N. Y.; Depasquale, S. E.; Nowara, E.; Gilbert, L.; Gersh, R. H.; Teneriello, M. G.; Harb, W. A.; Konstantinopoulos, P. A.; Penson, R. T.; Symanowski, J. T.; Lovejoy, C. D.; Leamon, C. P.; Morgenstern, D. E.; Messmann, R. A. PRECEDENT: A randomized phase II trial comparing vintafolide (EC145) and pegylated liposomal doxorubicin (PLD) in combination versus PLD alone in patients with platinum-resistant ovarian cancer. *J. Clin. Oncol.* **2013**, *31*, 4400−4406.

(13) Deng, Y.; Wang, Y.; Cherian, C.; Hou, Z.; Buck, S. A.; Matherly, L. H.; Gangjee, A. Synthesis and discovery of high affinity folate receptor-specific glycinamide ribonucleotide formyltransferase inhibitors with antitumor activity. *J. Med. Chem.* **2008**, *51*, 5052−5063.

(14) Kugel Desmoulin, S.; Wang, Y.; Wu, J.; Stout, M.; Hou, Z.; Fulterer, A.; Chang, M. H.; Romero, M. F.; Cherian, C.; Gangjee, A.; Matherly, L. H. Targeting the proton-coupled folate transporter for selective delivery of 6-substituted pyrrolo[2,3-*d*]pyrimidine antifolate inhibitors of de novo purine biosynthesis in the chemotherapy of solid tumors. *Mol. Pharmacol.* **2010**, *78*, 577−587.

(15) Wang, Y.; Cherian, C.; Orr, S.; Mitchell-Ryan, S.; Hou, Z.; Raghavan, S.; Matherly, L. H.; Gangjee, A. Tumor-targeting with novel non-benzoyl 6-substituted straight chain pyrrolo[2,3-*d*]pyrimidine antifolates via cellular uptake by folate receptor alpha and inhibition of de novo purine nucleotide biosynthesis. *J. Med. Chem.* **2013**, *56*, 8684−8695.

(16) Deng, Y.; Zhou, X.; Kugel Desmoulin, S.; Wu, J.; Cherian, C.; Hou, Z.; Matherly, L. H.; Gangjee, A. Synthesis and biological activity of a novel series of 6-substituted thieno[2,3-*d*]pyrimidine antifolate inhibitors of purine biosynthesis with selectivity for high affinity folate receptors over the reduced folate carrier and proton-coupled folate transporter for cellular entry. *J. Med. Chem.* **2009**, *52*, 2940−2951.

(17) Wang, L.; Cherian, C.; Desmoulin, S. K.; Polin, L.; Deng, Y.; Wu, J.; Hou, Z.; White, K.; Kushner, J.; Matherly, L. H.; Gangjee, A. Synthesis and antitumor activity of a novel series of 6-substituted pyrrolo[2,3-*d*]pyrimidine thienoyl antifolate inhibitors of purine biosynthesis with selectivity for high affinity folate receptors and the proton-coupled folate transporter over the reduced folate carrier for cellular entry. *J. Med. Chem.* **2010**, *53*, 1306−1318.

(18) Wang, L.; Kugel Desmoulin, S.; Cherian, C.; Polin, L.; White, K.; Kushner, J.; Fulterer, A.; Chang, M. H.; Mitchell-Ryan, S.; Stout, M.; Romero, M. F.; Hou, Z.; Matherly, L. H.; Gangjee, A. Synthesis, biological, and antitumor activity of a highly potent 6-substituted pyrrolo[2,3-*d*]pyrimidine thienoyl antifolate inhibitor with proton-coupled folate transporter and folate receptor selectivity over the reduced folate carrier that inhibits beta-glycinamide ribonucleotide formyltransferase. *J. Med. Chem.* **2011**, *54*, 7150−7164.

(19) Kugel Desmoulin, S.; Wang, L.; Hales, E.; Polin, L.; White, K.; Kushner, J.; Stout, M.; Hou, Z.; Cherian, C.; Gangjee, A.; Matherly, L. H. Therapeutic targeting of a novel 6-substituted pyrrolo [2,3-*d*]pyrimidine thienoyl antifolate to human solid tumors based on selective uptake by the proton-coupled folate transporter. *Mol. Pharmacol.* **2011**, *80*, 1096−1107.

(20) Cherian, C.; Kugel Desmoulin, S.; Wang, L.; Polin, L.; White, K.; Kushner, J.; Stout, M.; Hou, Z.; Gangjee, A.; Matherly, L. H. Therapeutic targeting malignant mesothelioma with a novel 6-substituted pyrrolo[2,3-*d*]pyrimidine thienoyl antifolate via its selective uptake by the proton-coupled folate transporter. *Cancer Chemother. Pharmacol.* **2013**, *71*, 999−1011.

(21) Wong, S. C.; Proefke, S. A.; Bhushan, A.; Matherly, L. H. Isolation of human cDNAs that restore methotrexate sensitivity and reduced folate carrier activity in methotrexate transport-defective Chinese hamster ovary cells. *J. Biol. Chem.* **1995**, *270*, 17468−17475.

(22) Flintoff, W. F.; Davidson, S. V.; Siminovitch, L. Isolation and partial characterization of three methotrexate-resistant phenotypes from Chinese hamster ovary cells. *Somatic Cell Genet.* **1976**, *2*, 245−261.

(23) Wang, L.; Cherian, C.; Kugel Desmoulin, S.; Mitchell-Ryan, S.; Hou, Z.; Matherly, L. H.; Gangjee, A. Synthesis and biological activity of 6-substituted pyrrolo[2,3-*d*]pyrimidine thienoyl regioisomers as inhibitors of de novo purine biosynthesis with selectivity for cellular uptake by high affinity folate receptors and the proton-coupled folate transporter over the reduced folate carrier. *J. Med. Chem.* **2012**, *55*, 1758−1770.

(24) Zhao, R.; Goldman, I. D. The molecular identity and characterization of a proton-coupled folate transporter—PCFT: Biological ramifications and impact on the activity of pemetrexed. *Cancer Metastasis Rev.* **2007**, *26*, 129−139.

(25) Webb, B. A.; Chimenti, M.; Jacobson, M. P.; Barber, D. L. Dysregulated pH: A perfect storm for cancer progression. *Nature Rev. Cancer* **2011**, *11*, 671−677.

(26) Rosowsky, A.; Bader, H.; Wright, J. E.; Keyomarsi, K.; Matherly, L. H. Synthesis and biological activity of N-omega-hemiphthaloyl-alpha,omega-diaminoalkanoic acid analogues of aminopterin and 3′,5-dichloroaminopterin. *J. Med. Chem.* **1994**, *37*, 2167−2174.

(27) Chen, C.; Ke, J.; Zhou, X. E.; Yi, W.; Brunzelle, J. S.; Li, J.; Yong, E.-L.; Xu, H. E.; Melcher, K. Structural basis for molecular recognition of folic acid by folate receptors. *Nature* **2013**, *500*, 486−489.

(28) Wibowo, A. S.; Singh, M.; Reeder, K. M.; Carter, J. J.; Kovach, A. R.; Meng, W.; Ratnam, M.; Zhang, F.; Dann, C. E. Structures of human folate receptors reveal biological trafficking states and diversity in folate and antifolate recognition. *Proc. Natl. Acad. Sci. U. S. A.* **2013**, *110*, 15180−15188.

(29) Zhang, Y.; Desharnais, J.; Marsilje, T. H.; Li, C.; Hedrick, M. P.; Gooljarsingh, L. T.; Tavassoli, A.; Benkovic, S. J.; Olson, A. J.; Boger,

D. L.; Wilson, I. A. Rational design, synthesis, evaluation, and crystal structure of a potent inhibitor of human GARTfase: 10-(Trifluoroacetyl)-5,10-dideazaacyclic-5,6,7,8-tetrahydrofolic acid. *Biochemistry* **2003**, *42*, 6043−6056.
(30) Kugel Desmoulin, S.; Wang, L.; Polin, L.; White, K.; Kushner, J.; Stout, M.; Hou, Z.; Cherian, C.; Gangjee, A.; Matherly, L. H. Functional loss of the reduced folate carrier enhances the antitumor activities of novel antifolates with selective uptake by the proton-coupled folate transporter. *Mol. Pharmacol.* **2012**, *82*, 591−600.
(31) Moran, R. G.; Colman, P. D.; Rosowsky, A. Structural requirements for the activity of antifolates as substrates for mammalian folylpolyglutamate synthetase. *NCI Monogr.* **1987**, 133−138.
(32) Moran, R. G.; Colman, P. D.; Rosowsky, A.; Forsch, R. A.; Chan, K. K. Structural features of 4-amino antifolates required for substrate activity with mammalian folylpolyglutamate synthetase. *Mol. Pharmacol.* **1985**, *27*, 156−166.
(33) *LeadIT 2.1.6*; BioSolveIT GmbH: Sankt Augustin, Germany, 2013; www.biosolveit.de.
(34) *Molecular Operating Environment (MOE)*, 2013.08; Chemical Computing Group Inc.: 1010 Sherbooke St. West, Suite #910, Montreal, QC, Canada, H3A 2R7, 2013.
(35) McNicholas, S.; Potterton, E.; Wilson, K. S.; Noble, M. E. M. Presenting your structures: The CCP4mg molecular-graphics software. *Acta Crystallogr., Sect. D: Biol. Crystallogr.* **2011**, *67*, 386−394.
(36) Lowry, O. H.; Rosebrough, N. J.; Farr, A. L.; Randall, R. J. Protein measurement with the folin phenol reagent. *J. Biol. Chem.* **1951**, *193*, 265−275.